p-ISSN 2655-9145
e-ISSN 0000-0000

JAMETECH

Journal of
APPLIED MECHANICAL ENGINEERING AND GREEN TECHNOLOGY

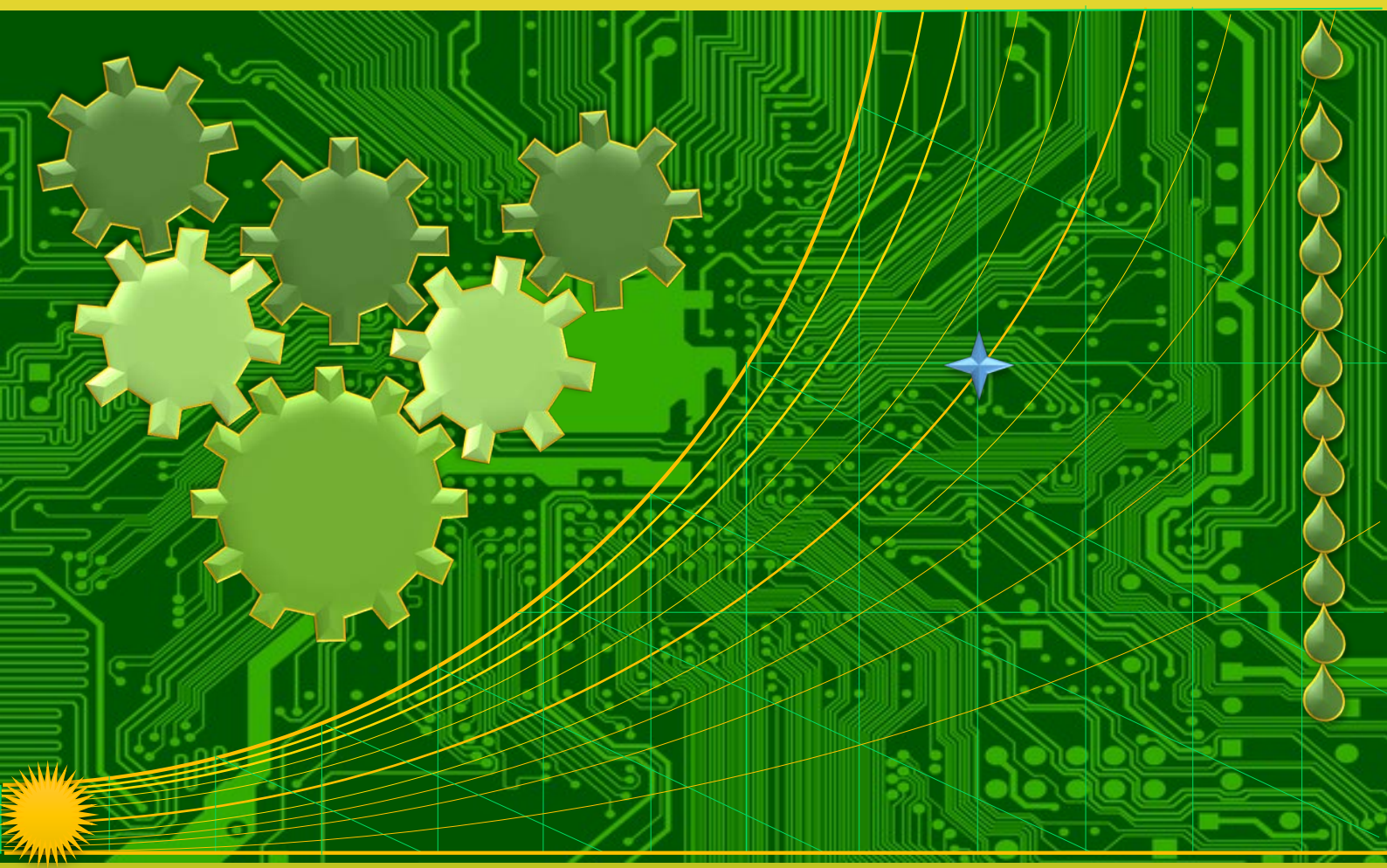

JAMETECH | Volume 1 | Number 1 | Pages 1-40 | March 2019

JAMETECH

Journal of
APPLIED MECHANICAL ENGINEERING AND GREEN TECHNOLOGY

Gedung P3M, Lt.1 Politeknik Negeri Bali, Bukit Jimbaran
PO BOX 1064, Kuta Selatan, Badung, Bali - Indonesia
Telp. (+62)361 701981 Fax. (+62)361 701128
Email: jametech@pnb.ac.id

JOURNAL TEAM

PREFACE

Journal of Applied Mechanical Engineering and Green Technology promotes and enhances research developments and publication of original research papers, review articles, short reports and experimental details. It is essential reading for all those wishing to keep well informed of research and industrial news in the fields of Applied Mechanical Engineering and Green Technology. The journal also provides platforms for debate and dissemination of research findings whilst also facilitating the discussion of new research areas and techniques.

The scope of the journal encompasses research into broad aspects in Mechanical Engineering, Green Technology and associated fields include Mechanics, Materials, Manufacturing and Production, Design and Construction, Automotive, Refrigeration Heating Ventilating and Air Conditioning (RHVAC), Mechanical and Plumbing for Buildings, Sustainable Energy Management and Technology, New, and Renewable Energy Technologies. This is particularly important in these times of rapid introduction of alternative new and renewable energy sources and the emergence of new sustainable energy technology. The journal also brings the development of new research approaches in the area.

The journal is managed by Department of Mechanical Engineering and published by the Center of Research and Community Services of Politeknik Negeri Bali three times in a year: March, July and November. Papers in this journal are published in English.

Best Regards,
JAMETECH Editorial Team

TABLE OF CONTENTS

Journal of Applied Mechanical Engineering and Green Technology

Journal homepage: http://ojs.pnb.ac.id/index.php/JAMETECH
p-ISSN: 2655-9145; e-ISSN: 0000-0000

Numerical simulations on evaporator coils of sustainable cold storages for food chain application

I.N. Suamir[a1], I.M. Rasta[a], A. Winarta[a] and I.W. Suirya[a]

[a]*Mechanical Engineering Department, Politeknik Negeri Bali, Campus Street Bukit Jimbaran, Kuta Selatan, Bali 80364, Indonesia*

Abstract

The development of cold storage in Indonesia is less than satisfactory. As the second highest producers of fishery and aquaculture products in the world, the country has only 2 out of total 6 of its ocean fishing ports possess cold storage facilities. Indonesia is also on the list of low index cold storage markets with abundant natural resources. The lack of cold storage facilities has greatly restricted the development of its fishery and food industries. The current infrastructure is also too poor to exploit the resources efficiently. Under this circumstance, technologies that can encourage development of sustainable cold storages applied for food chain and related components such evaporator coils in the country is in great demand. To date there has not been much research into cold storage evaporator coil design specifically for natural refrigerants such as Hydrocarbon (HC) and CO_2. This paper presents results of theoretical investigation on the main design parameters of natural refrigerant evaporator coils which can be applied in sustainable cold storage systems. The parameters included tube diameter, number of refrigerant circuits, evaporator temperature and circulation ratio. A lumped element technique was applied to develop evaporator models which were used to design and to simulate different coil geometry and circuit arrangements. The results from published papers were used for model validation. The evaporators considered were direct expansion and flooded evaporator coils for low temperature cold storage applications. The paper also presents comparison analyses of natural refrigerant (HC and CO_2) evaporator coils and direct expansion coils using the synthetic refrigerant R-404A.

Keywords: Evaporator coil; natural refrigerants; sustainable cold storage; performance analyses

1. Introduction

Indonesia is an agriculture country with population number of 258.5 million. Poultry, beef and veal production are anticipated to increase 3 to 5 percent annually through 2020, while consumption is expected to rise 4 to 6 percent annually [1]. The country has experienced unbalanced food supply and demand which may need to be well-adjusted through import policy. As an example, beef supply of the country in 2016 was estimated 348,020 tons, while the demand was 651,420 tons [2]. Unbalanced food supply will boost the price of food, sometimes reaching unreasonable level which very much affects the lives of low income populations. This is one of the challenges for the country in improving food security and sustainability.

Furthermore, FAO [3] stated that Indonesia is the second highest producers of fishery and aquaculture products in the world. Fishery and aquaculture production of the country in 2014 was 14.33 million tons. In 2016, the production reached 23.03 million tons which 27.6% came from marine fisheries and 72.4% from aquaculture [4]. Additionally, Indonesian territory consists of 2/3 of water, has given enormous benefits for Indonesia, especially fishermen. To improve the economic level of fishermen requires efforts to develop proper facilities. One of the efforts is by improving the quality of products which can be marketed in the regional and international levels. It is certainly need the support of the existence of various fishery facilities, one of which is cold storage [5].

The development of cold storage for fishery industry in Indonesia is less than satisfactory. As the second highest producers of fishery and aquaculture products in the world, the country has only 2 out of total 6 of its ocean fishing ports possess cold storage facilities. Moreover, only 4 out of total 14 national fishery ports own cold storage facilities [5]. Indonesia is also on the list of low index cold storage markets with abundant natural resources [1]. The lack of cold storage facilities has greatly restricted the development of its fishery industry. The current infrastructure is also too poor to exploit the resources efficiently. Under this circumstance, technology that can encourage development

[1]Corresponding author. Tel.: +6281237594781; Fax: +62361702811
E-mail address: nyomansuamir@pnb.ac.id

Nomenclature

A	Area (m^2)	*Greek symbols*	
Cp	Specific heat (kJ kg^{-1} $^oC^{-1}$)	δ	
CR	Circulation ratio	η	Thickness
d	Diameter (m)	θ	Efficiency
EC	Evaporator coil	λ	Dry angle
DX	Direct expansion	ρ	Conductivity (kW m^{-1} $^oC^{-1}$)
G	Mass velocity (kg s^{-1} m^{-2})	ω	Density (kg m^{-3})
H	Enthalpy (kJ kg^{-1})	*Subscript*	Humidity ratio (kg kg_{da}^{-1})
j	Colburn j-factor	a	air; air side
h	Heat transfer coefficient (kW m^{-2} $^oC^{-1}$)	c	convective
LT	Low temperature	cb	convective boiling
MT	Medium temperature	e	evaporator
m	Mass (kg); mass flow rate (kg s^{-1})	f	fin
N	Number of rows	i	in; width axis
P	Pressure (kPa)	j	depth axis
Pr	Prandtl number	k	height axis
Q	Refrigeration load (kW)	lat	latent
Re	Reynold number	nb	nucleate boiling
RH	Relative humidity	o	out
S	Suppression factor (m)	r	refrigerant
T	Temperature (^oC)	sp	single phase
t	Time (s)	tp	two phase
U	Overall heat transfer coefficient (kW m^{-2} $^oC^{-1}$)	v	vapor

of infrastructure including cold storage in the country is in extremely great demand.

The demand for refrigerated facilities such as refrigerated warehouse, cold storage and retail refrigeration in Indonesia is expected to increase with the country's economic development because they have a vital role to play in reducing post-harvest losses, improving quantity and quality of fishery and aquaculture products and maintain food supply to consumers. The facilities enable to store over supply of foodstuffs during crop season and use them when there are no crops. The refrigerated facilities are also essential for food quality preservation. However, the increase of refrigerated facilities can provide impact to the environment due to refrigerant leakage and energy use. It has been well-known that refrigeration systems consume intensive energy.

The use of natural refrigerants such as CO_2 and Hydrocarbon offers the opportunity to reduce not only the direct impacts of systems employing HFC refrigerants that possess high global warming potential but also the indirect impacts by improving energy efficiency. Another advantage of CO_2 over HFC refrigerants is its better heat transfer properties that can lead to an increase in the evaporating temperature. A consequence of this is a potential increase in the refrigeration capacity of the coil and a reduction in the rate of frost formation on the coil surface.

Supermarkets have two refrigeration temperature levels, medium temperature (MT) and low temperature (LT) refrigeration. Evaporating temperature of MT refrigeration system is -8^{o}C and -30^{o}C for LT refrigeration system. The refrigeration systems employed can be direct expansion or of the secondary loop type. In conventional supermarkets, the direct expansion refrigeration system is the most commonly used to provide refrigeration to display cabinets located in the store. For supermarkets which have used natural refrigerants such as CO_2, the applications of secondary refrigeration loops are of particular interest. As CO_2 has low viscosity, the use of CO_2 refrigerant as volatile secondary fluid can significantly improve the performance of the refrigeration system due to its small pumping power. Analyses on secondary loop refrigeration systems using CO_2 as secondary fluid has been reported by [6,7].

Finned tube heat exchangers are commonly used as forced air evaporators of display cabinets in supermarkets. Performance of the evaporator coil directly affects the temperature performance of a display cabinet and the overall performance of the supermarket refrigeration system. The influences of geometry and configuration of finned tube coils using synthetic refrigerants have been intensively investigated by many researchers. Romero-Mendez et al. [8] investigated the effects of fin spacing to the hydrodynamics and heat convection of a plate fin and tube heat exchanger. Liang et al. [9] and Jiang et al. [10] showed the impacts of circuiting on performance and parameter distributions within the tubes and across the coil. Getu and Bansal [11] developed a model of R-404A evaporator coil to analyze the performance of the coils in LT supermarket display cabinets. Chandrasekharan and Bullard [12] developed a design tool for a fin and tube display cabinet evaporator to predict local and overall effects of frost accumulation.

To date there has not been much research into evaporator coil design specifically for CO_2 refrigerant. Aidoun and Ouzzane [13] established a numerical model to study the effects of circuitry of CO_2 finned tube evaporators and found that it was possible to use longer circuits, thus reducing the number of circuits for a given refrigeration capacity. Authors in [14,15] investigated the impact of the

geometry, tube circuitry and tube diameter on the performance of CO_2 evaporators and showed that by reducing the number of circuits could increase the velocity of refrigerant and reduce the total length of pipe. This study investigated the performance of CO_2 evaporator coils under different geometry, circuitry arrangement and different operating conditions for chilled food and frozen food display cabinets in supermarket applications. Comparison analyses with evaporator coils using R-404A refrigerant were also performed.

Supermarket refrigeration systems using HFC refrigerants are responsible for substantial greenhouse gas emissions from leakage of refrigerant to the ambient and indirect emissions from the electrical power used by the compressors, fans and other ancillary equipment [16]. Direct emissions from refrigerant leakage can sometimes be as high as indirect emissions, and for this reason, legislation at has been aimed at effecting reductions in direct emissions. Another way to significantly reduce or completely eliminate direct emissions is through the use of natural refrigerants, such as hydrocarbons, CO_2 and ammonia. In recent years, considerable research has been carried out on the development and application of supermarket refrigeration systems employing natural refrigerants. Most systems deployed in the field are either trans-critical 'booster' CO_2 systems, cascade all CO_2 systems, or subcritical CO_2 systems cascaded with a hydrocarbon system on the high pressure side for heat rejection [17,18,19].

An interesting approach developed and applied by some supermarket chains involves the use of 'integral' hydrocarbon cabinets with heat rejection to the air in the supermarket [20] and combination of heat rejection to the air as well as water in a closed loop system [21]. The heat in the water circuit can be either upgraded through a boiler or heat pump and used for domestic hot water and/or space heating, or rejected to the ambient through a dry cooler. This approach can provide energy integration between the refrigeration and space conditioning systems in the store and offers the potential for energy savings if the system is appropriately designed and controlled.

2. Numerical Model Approach

2.1. Numerical models

Three main numerical models were established to investigate the performance of CO_2 and HC evaporator coils under different geometry, circuit arrangement and different operating conditions. The first model was for the investigation of the performance of MT CO_2 flooded evaporator coil. The second model was for the simulation of the performance of CO_2 DX evaporator coils for both chilled and frozen temperature levels. The third model was for HC (R-1270) DX evaporator coil. The additional model was also developed to analyze the coil performance using refrigerant R-404A for comparative analyses. The models can also be used to design the geometry and tube arrangement of evaporator coils for a given refrigeration capacity. The numerical models apply standard plate fin specification from [22] to determine fin and tube pattern, height and width of the coil. The models were developed using the software EES.

To simulate the flooded and DX evaporator coils, some main assumptions were made as follows: steady state flow conditions; one dimensional flow for refrigerant inside tubes and air across the coil; negligible thermal losses to the environment; uniform temperature and air flow; constant air side convective heat transfer coefficient over the entire coil; intermediate pressure (P_{int}) to be considered as condensing pressure for CO_2 DX evaporator coil, negligible refrigerant pressure drops of less than 2 K saturated temperature equivalent for DX coils [22] and less than 1 K for flooded coils; the same number of tubes in each circuit with the same fraction of total mass flow rate; quasi steady frosting process; maximum pressure drop at air side after frost to be lower than 0.175 kPa.

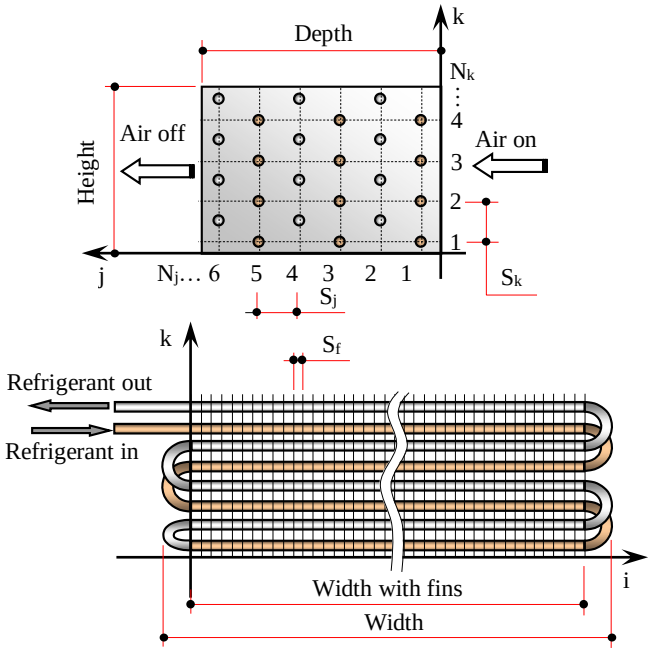

Figure 1. Geometry of a finned tube evaporator model

To simulate the geometry and circuitry of the evaporator coils, certain assumptions were made as follows: constant air side convective heat transfer coefficient over the entire coil; condensing pressure of 12.7 bar_a (corresponds to 29 ºC condensing temperature), evaporating temperature of -7 ºC; negligible refrigerant pressure drop of less than 2 K saturated temperature drop equivalent; the same number of tubes in each circuit with the same fraction of total mass flow rate; quasi steady frosting process; maximum pressure drop at air side after frost to be lower than 0.175 kPa.

The mathematical modeling approach and design strategy for the coil followed the process described by [15]. The evaporation heat transfer coefficient for refrigerant R1270 was determined from the correlation by [23]. The two phase pressure drop was calculated from [24,25]. The heat transfer coefficient and pressure drop correlations were associated with the flow pattern map developed by [26].

Figure 1 shows the basic geometry of the finned tube evaporator considered in the models. The tubes are arranged in coordinates along width, depth and height axes (i, j, k) as can be seen in the figure. The number of rows and tube pattern can be used to determine the size of the coil and the tube interconnections within the coil circuits. If the coil has more than one circuit, the number of tubes in each circuit should be evenly balanced.

The mathematical models used the lumped element technique by which the evaporator coil can be divided into

the superheated and two phase regions. A DX coil has two lumped regions (single and two phase regions), while a flooded evaporator coil only has a one region, the two phase region as shown in Figure 2. Each region is considered as a single control volume. The fraction of the coil area in each control volume in a DX coil is calculated in proportion to the amount of heat transfer in each control volume.

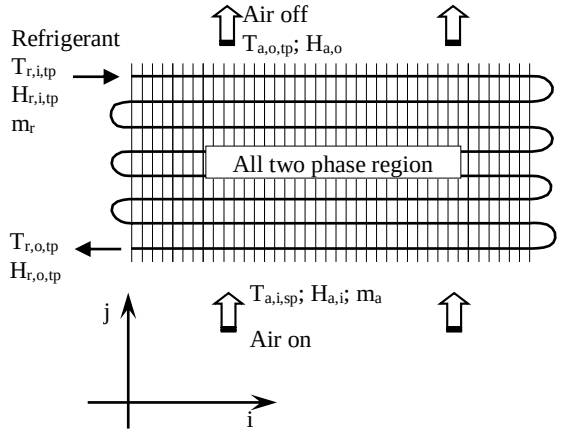

a) Flooded coil with single lumped region

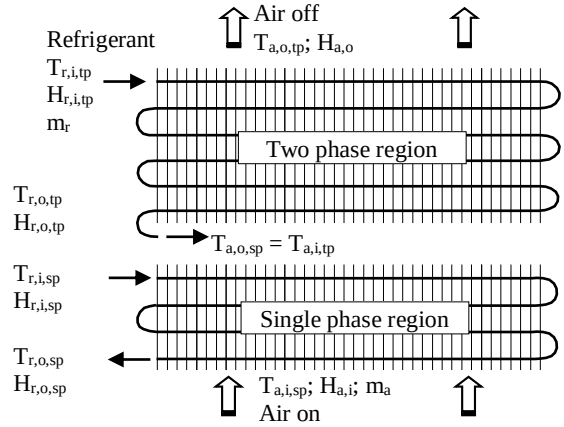

b) Direct expansion coil with two lumped regions

Figure 2. Schematic of flooded and DX evaporator coils with single and two control volumes

The mass and energy balance principles are applied to each control volume, which is summarized in equations (1) to (3). For the flooded evaporator coil, a single phase region does not exist, thus the heat transfer rate component for single phase region ($Q_{r,sp}$) is omitted. ΔT_{lm} is the logarithmic mean temperature difference of each control volume. The air side surface area of the coil (A_a) and other geometric parameters of the coil such as free flow area and free flow area with frost were calculated as in [27].

$$Q_e = Q_{r,tp} + Q_{r,sp} = Q_a \tag{1}$$

$$Q_e = m_r\,(h_{r,o,tp} - h_{r,i,tp}) + m_r\,(h_{r,o,sp} - h_{r,i,sp}) = m_a\,(h_{a,i} - h_{a,o}) \tag{2}$$

$$Q_e = U_{a,tp} A_{a,tp} \Delta T_{lm,tp} + U_{a,sp} A_{a,sp} \Delta T_{lm,sp} \tag{3}$$

The overall heat transfer coefficient (U_a) of the coil with frost can be calculated from equation (4). For frost free coil the component of frost resistance is not included. For the DX coil the external and internal heat transfer areas as well as the internal heat transfer coefficient depend on the mode of heat transfer, single or two phases.

$$\frac{1}{U_a} = \frac{1}{\eta_f h_a} + \frac{\delta_{frost}}{\eta_f \lambda_{frost}} + \frac{A_a \ln\left(\frac{d_o}{d_i}\right)}{2\pi\lambda_t L_r} + \frac{A_a}{A_r h_r} \tag{4}$$

2.2. Correlations of heat transfer coefficient and pressure drop at refrigerant side

The local heat transfer coefficient and pressure drop for the two phase flow of CO_2 were calculated using the correlations reported by [28,29,30]. The correlations for the two-phase frictional pressure drop for CO_2 were based on the correlations proposed by [24,25].

The local heat transfer coefficients and pressure drop correlations were selected for each flow regime as it changes with the flow and evaporation of refrigerant in the evaporator. Thus the correlations reliably capture the variation of two phase heat transfer coefficient and frictional pressure drops at different mass velocities and vapor qualities.

Equations (5) and (6) show the general equations for the two phase heat transfer coefficient and pressure drop on the refrigerant side of the evaporator. The detailed correlations for each flow regime and for the single phase region can be found in [29,30].

$$h_{tp} = \frac{\theta_{dry} h_v + (2\pi - \theta_{dry})\left[\left(Sh_{nb}\right)^3 + h_{cb}^3\right]^{(1/3)}}{2\pi} \tag{5}$$

$$\Delta P_{total} = \Delta P_{static} + \Delta P_{momentum} + \Delta P_{frictional} \tag{6}$$

The evaporation heat transfer coefficient for refrigerant R-404A was determined from the correlation by [23]. The two phase pressure drop was calculated from [24,25]. The heat transfer coefficient and pressure drop correlations were associated with the flow pattern map developed by [26].

2.3. Correlations of heat transfer coefficient and pressure drop on the air side

Air side convective heat transfer coefficient has been calculated using the Colburn j-factor proposed by [31], while the total heat transfer coefficient for wet coil and pressure drop were calculated based on the equations by [11]. The air side heat transfer coefficient can be calculated from:

$$h_a = h_{c,a} + h_{lat,a} \tag{7}$$

$$h_{c,a} = \frac{j\,Cp_a\,G_a}{\mathrm{Pr}^{2/3}} \tag{8}$$

2.4. Calculation of frost accumulation

Frost accumulation on the evaporator surface has been estimated using the method proposed by [11]. The rate of frost accumulation was determined from equation (9) and the amount of frost accumulated on the surface of the evaporator and frost thickness after Δt time, from equation (10).

$$m_{frost} = m_a\,(\omega_i - \omega_o) \tag{9}$$

$$\Delta m_{frost} = m_{frost}\Delta t \qquad \text{and} \qquad \delta_{frost} = \frac{\Delta m_{frost}}{\rho_{frost} A_a} \tag{10}$$

Detailed calculations of density, thermal conductivity and diffusivity of the frost can be found in [11].

3. Results and Discussion

Test results from the experimental CO_2 test facility were used to validate the models. The model of conventional evaporator coil with R-404A was validated against data provided by the manufacturer. Comparison between predictions and experiments under design conditions was found to be satisfactory for the refrigeration capacity as shown in Table 1. The pressure drop estimations were, however, lower than the experiment results mainly because the pressure drops across the distributor and lead tubes were not included in the model. For synthetic refrigerants these pressure drops can be as high as 89% of total pressure drops in the evaporator coil [32].

The validated models were used to design 8 evaporator coils with different geometry and circuitry. The evaporator coils were simulated at evaporating temperature of -8 ºC for MT coils and -30 ºC for LT coils. Tubes and fins were made from copper and aluminum respectively. Equilateral fin and tube pattern in a staggered arrangement was applied. The temperature of chilled food display cabinet was in the range of -1 to 1 ºC and frozen food display cabinet was in the range of -19 to -21 ºC.

Table 1. Numerical model and experimental results

Parameters		[a] MT CO_2 Models		[b] DX LT CO_2 model	[c] DX R-404A model
		Flooded	DX		
Q_e (kW) full load, ΔT_a = 10 K	Model/ Experiment	5.19 5.10	5.09 4.93	3.00 2.89	- -
Q_e (kW) steady state load, ΔT_a = 9 K for MT and ΔT_a = 8 K for LT	Model Experiment	4.55 4.42	4.46 4.30	2.35 2.12	3.65 3.60*
ΔP_r (kPa) steady state	Model Experiment	11.31 21.15	9.22 16.87	6.01 14.87	40.92 148.28*

Evaporator coil investigated:
[a] Tube arrangement: staggered; d_o = 12.70 (mm); N_k = 4; N_j = 6; number of circuits = 4; fins pitch 4 fins/inch
[b] Tube arrangement: staggered; d_o = 12.70 (mm); N_k = 4; N_j = 8; number of circuits = 3; fins pitch 3 fins/inch
[c] Tube arrangement: inline; d_o = 15.87 (mm); N_k = 2; N_j = 16; number of circuits = 2; fins pitch 3 fins/inch
* Data from manufacturer

Table 2 shows the geometry of the evaporator coils together with their performance parameters. It can be seen the physical sizes of the CO_2 evaporator coils are varied and are generally much smaller compared to the coils with R-404A. For the given refrigeration duty, the flooded MT coil with tube diameter 9.52 mm (EC-3) has the smallest size with refrigerant volume about 62% of the MT DX coil using the same tube diameter (EC-1) and about 19% of that in the R-404A evaporator coil (EC-5).

Table 2. Geometry of the designed coils with their performance parameters

Parameters	MT evaporator coils					LT evaporator coils		
	DX CO_2		Flooded CO_2		DX R-404A	DX CO_2		DX R-404A
	EC-1	EC-2	EC-3	EC-4	EC-5	EC-6	EC-7	EC-8
Tube outside diameter (mm)	9.52	12.70	9.52	12.70	15.87	9.52	12.70	15.87
Number of rows high	2	2	2	2	2	2	2	2
Number of rows deep	21	17	13	10	20	12	10	12
Number of circuits	2	1	2	1	2	2	1	2
Total tube length (m)	91.1	73.8	56.4	43.4	86.6	48.7	40.6	48.7
Height (mm)	63.5	63.5	63.5	63.5	76.2	63.5	63.5	76.2
Depth (mm)	577.4	467.4	357.5	275.0	659.9	330.0	275.0	395.9
Width with fins (mm)	2170	2170	2170	2170	2170	2030	2030	2030
Refrigerant volume (L)	4.14	6.78	2.56	3.99	13.47	2.22	3.74	7.57
G_r (kg s^{-1} m^{-2})	171.0	168.7	199.8	198.1	109.0	100.4	99.0	72.2
CR	-	-	1.2	1.2	-	-	-	-
Q_e (kW)	3.75	3.75	3.75	3.76	3.76	2.25	2.25	2.25
$Q_{e,frost}$ (kW)*	3.26	3.12	3.24	2.96	3.44	2.16	2.14	2.15
Fin efficiency	0.85	0.88	0.85	0.88	0.87	0.89	0.92	0.90
h_r (kW m^{-2} $ºC^{-1}$)	2.899	3.107	3.206	3.473	0.482	2.521	2.802	0.337
h_a (kW m^{-2} $ºC^{-1}$)	0.062	0.073	0.064	0.075	0.063	0.042	0.050	0.046
ΔP_r (kPa)	65.13	30.89	42.34	19.27	50.47	33.15	16.24	31.79
$\Delta P_{a,frost}$ (kPa)	0.016	0.024	0.030	0.043	0.013	0.018	0.020	0.010

The CO_2 coils also need less refrigerant charge as shown in Fig. 3, assuming 25% and 35% of the evaporator volume was filled with liquid for the DX and flooded evaporator coils respectively.

The CO_2 evaporator coils with smaller tube diameter require more tube rows and longer tubes to meet the designed refrigeration duty. Using single circuit arrangement results in high pressure drop particularly for the DX type coils. As can be seen in Table II the pressure drops of the CO_2 coils (EC-1, EC-3 and EC-6) are still higher than the coils with larger tube diameter (EC-2, EC-4 and EC-7) even in two circuit arrangement. The pressure drop will be higher if the pressure drop across the distributor and lead tubes is taken into account. Moreover, the physical size of the coils, except for in the case of the flooded coil EC-3, is larger which may increase their production cost.

Figure 4 shows the performance variation of CO_2 MT DX coils with evaporating temperature. Increasing the evaporating temperature can slightly improve the refrigeration capacity and reduce the pressure drop. Similar effect was also found on the LT DX and flooded evaporator coils. In Figures 5 and 6, the performance of the flooded CO_2 evaporator coils at different circulation ratios (CR) is shown.

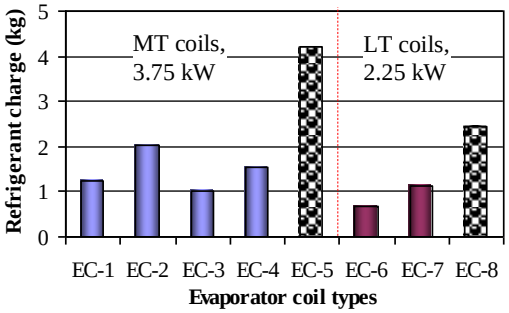

Figure 3. Refrigerant charge comparisons

As the CR increases, the refrigeration duty slightly improves due to the enhancement of the evaporation heat transfer coefficient. However, the increase of the CR considerably increases the pressure drop and refrigerant mass velocity which increases the power consumption of the CO_2 pump and causes a reduction in the coefficient of performance of the refrigeration system. The CR, therefore, should be chosen to be as low as possible in the range of the designed refrigeration capacity. The experimental tests showed the optimum CR to be in the range 1.1 and 1.3.

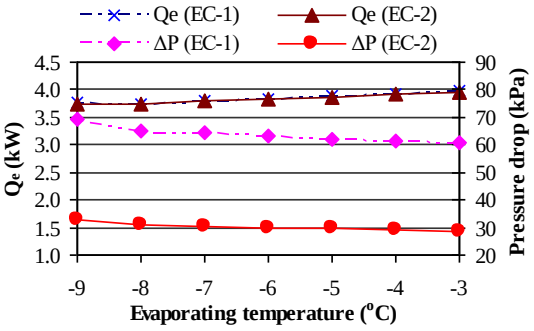

Figure 4. The influence of evaporating temperature

Numerical models have been developed and validated for design and performance simulation of finned tube flooded and direct expansion coils. Different geometry and circuitry arrangements were simulated using CO_2 and R-404A as refrigerants. The investigation found that for a given refrigeration capacity, CO_2 evaporator coils had considerably smaller size and lower refrigerant charge compared to the coils using R-404A refrigerant.

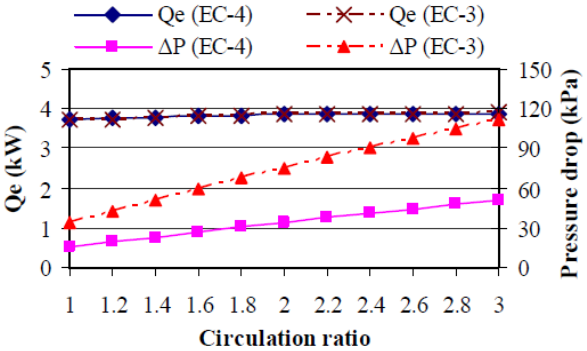

Figure 5. Refrigeration duty and pressure drops with circulation ratio (CR)

The investigation among the CO_2 evaporator coils showed that for the refrigeration capacity examined, using the larger tube diameter, the CO_2 DX evaporator coils were found to be more compact due to smaller number of rows along the depth of the oil. The pressure drop of the coils was also found to be lower. However, the coil had more refrigerant charge compared to the coil with the smaller tube diameter. For the CO_2 flooded evaporator application, the use of smaller tube diameter was found to be more favorable in terms of coil size and refrigerant charge.

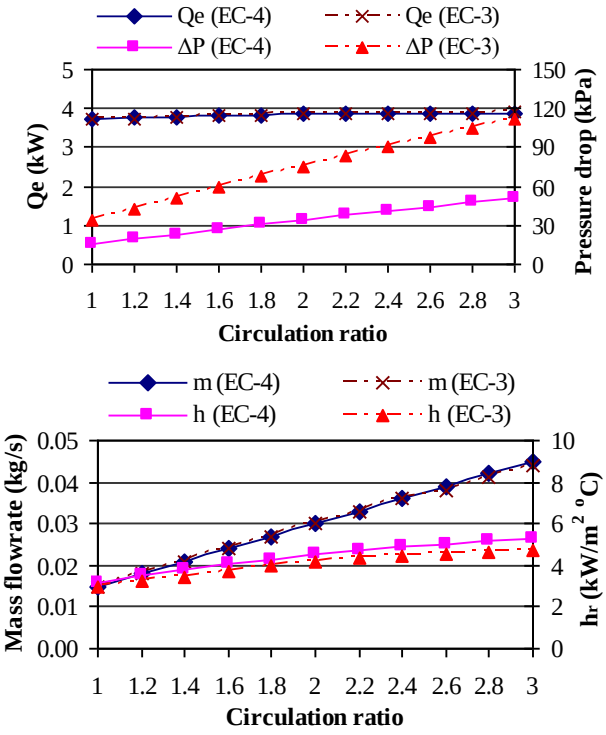

Figure 6. Refrigerant mass flow rate and heat transfer coefficient with circulation ratio

Table 3. Geometry of the designed coil with its performance parameters

Parameters	R1270 coil	R404A coil
Tube outside diameter (mm)	12	12
Number of rows high	2	2
Number of rows deep	10	14
Number of circuits	2	2
Total tube length (m)	70	98
Height (mm)	70	70
Depth (mm)	350	490
Width with fins (mm)	3500	3500
Refrigerant volume (L)	7.1	7.8
Refrigerant charge (kg)+	0.640	2.438
G_r (kg s^{-1} m^{-2})	67.66	206.1
Q_e (kW)	4.2	4.2
$Q_{e,frost}$ (kW)*	3.4	3.6
Fin efficiency**	0.83	0.84
h_r (kW m^{-2} $°C^{-1}$)	0.738	1.318
h_a (kW m^{-2} $°C^{-1}$)	0.052	0.048
ΔP_r (kPa)	8.53	97.38
$\Delta P_{a,frost}$ (kPa)*	0.016	0.010

* After frost accumulation of 240 minutes
**Fin thickness: 0.2 (mm); Fin pitch: 8 (mm) for R1270 and 10 (mm) for R404A
\+ Assumption 25% of the coil volume filled with liquid refrigerant.

Table 3 details the geometry of the R-1270 evaporator and original R-404A coil together with performance parameters obtained from the EES model. Because the R-1270 refrigeration system is comprised of two circuits, the coil geometry given in the table is for only one circuit. Similar assumptions were made for the R-404A coil. A 7 ºC superheat was also assumed for both coils. The results show that for the same load the R-1270 coil would require 70 m of copper pipe and 0.64 kg of refrigerant charge compared to 98 m pipe for the R-404A coil and 2.44 kg of refrigerant charge.

4. Conclusions

Numerical models have been developed and validated for design and performance simulation of finned tube flooded and direct expansion coils which can be applied in sustainable cold storage systems. Different geometry and circuitry arrangements were simulated using natural refrigerant CO_2 and Hydrocarbon (HC). For comparison simulation also performed for R-404A evaporator.

The investigation found that for a given refrigeration capacity, CO_2 evaporator coils had considerably smaller size and lower refrigerant charge compared to the coils using R-404A refrigerant. The investigation among the CO_2 evaporator coils showed that for the refrigeration capacity examined, using the larger tube diameter, the CO_2 DX evaporator coils were found to be more compact due to smaller number of rows along the depth of the coil.

The pressure drop of the coils was also found to be lower. However, the coil had more refrigerant charge compared to the coil with the smaller tube diameter. For HC evaporator coil, the results showed that, at the same refrigeration load, the HC coil would require 40% shorter copper pipe and 30% refrigerant charge compared to R404A evaporator coil.

Acknowledgment

The authors acknowledge the financial support received from the Higher Education Directorate General of the Ministry of Education and Culture of the Republic of Indonesia.

References

[1] J. Miller, "Top Markets Report Cold Chain, International Trade Administration," 2016, available from: http://trade.gov/topmarkets/pdfCold_Chain_Executive_Summary.pdf

[2] BPS, "Peternakan dalam angka-2016. Badan Pusat Statistik (Statistics Indonesia)," Jakarta, 2016, p. 101

[3] FAO, "The State of World Fisheries and Aquaculture 2016. Contributing to food security and nutrition for all," Rome, 2016, p. 200.

[4] MMAF-RI, "Capture and aquaculture production 2012-2016. Ministry of Marine Affairs and Fisheries Republic of Indonesia," 2016, available from: http://statistik.kkp.go.id/ sidatik-dev/2.php?x=2

[5] I.M. Putri and D.R. Munaf, "Increasing fishery economic added value through post fishing program: Cold storage program," International Journal of Social, Behavioral, Educational, Economic, Business and Industrial Engineering, 7, 2013, pp. 2391-2394

[6] S.W. Inlow and E.A. Groll, "Analysis of secondary loop refrigeration systems using carbon dioxide as volatile secondary refrigerant," HVAC&R Research, 2, 1996, pp. 107–120.

[7] A. Melinder and E. Granryd, "What to consider when using secondary fluids in indirect systems, Proc. Sustainable Refrigeration and Heat Pump Conference, Sweden, 2010, p. 12

[8] R. Romero-Mendez, M. Sen, K.T. Yang, R. McClain, "Effect of fin spacing on convection in plate fin and tube heat exchanger," Int. J. Heat and Mass Transfer, 43, 2000, pp. 39-51.

[9] S.Y. Liang, T.N. Wong, G.K. Nathan, "Numerical and experimental studies of refrigerant circuitry of evaporator coils," Int. J. Refrig., 24, 2001, pp. 823-833.

[10] H. Jiang, V. Aute, R. Radermacher, "Coil designer: a general-purpose simulation and design tool for air-to-refrigerant heat exchangers," Int. J. Refrig., 29, 2006, pp. 601-610.

[11] H.M. Getu and P.K. Bansal, "Modelling and performance analyses of evaporators in frozen-food supermarket display cabinets at low temperatures," Int. J. Refrig., 30, 2007, pp. 1227-1243.

[12] R. Chandrasekharan, P. Verma, C.W. Bullard, "Development of a design tool for display case evaporators," Int. J. Refrig., 29, 2006, pp. 823-832.

[13] Z. Aidoun and M. Ouzzane, "A model application to study circuiting and operation in CO2 refrigeration coils," Appl. Therm. Eng., 29, 2009, pp. 2544-2553.

[14] J.A. Shilliday and S.A. Tassou, "Numerical analysis of a plate fin and tube evaporator using the natural refrigerant CO_2," Proc. 1st IIR International cold chain conference, Sustainability and the Cold Chain, Cambridge, 2010.

[15] I.N. Suamir and S.A. Tassou, "Modeling and performance analyses of CO_2 evaporator coils for chilled and frozen food display cabinets in supermarket applications," Proc. International Congress of Refrigeration, Prague, 2011, p. 8.

[16] S.A. Tassou, J.S. Lewis, Y.T. Ge, A. Hadawey, I. Chaer, "A review of emerging technologies for food refrigeration applications," Appl. Therm. Eng., 30, 2010, pp. 263-276.

[17] S. Girotto, S. Minetto, P. Neksa, "Commercial refrigeration system using CO2 as the refrigerant," Int. J. Refrig., 27, 2004, pp. 717-723.

[18] A. Campbell, G.G. Maidment, J.F. Missenden, "A natural refrigeration system for supermarkets using CO2 as a refrigerant," Proc. CIBSE National Conference, London, 2006.

[19] D. Hinde, S. Shitong Zha, L. Lan, "Carbon dioxide in North American supermarkets,". ASHRAE Journal, 51,2009, pp. 18-26.

[20] Lidl, "Two hundred Lidl stores to feature R290 technology by 2012, 2011, available from: http://www.hydrocarbons21.com//content/articles/2011-01-14-200-lidl-stores-to-feature-r290-technology-by-2012.php.

[21] J. Gartshore, and S. Benton, "Cool concerns and Waitrose to support the use of hydrocarbons," 2010, available from: http://www.hydrocarbons21.com/content/articles/2010-07-22-cool-concerns-and-waitrose-to-support-the-use-of-hydrocarbons.php.

[22] SRC, "Standard plate fin coil specifications," 2010, available from: http://www.srcoils.com/wp-content/blogs.dir/1/files/2010/05/Coil_Specs_Nomenclature.pdf

[23] L. Wojtan, T. Ursenbacher, J.R. Thome, "Investigation of flow boiling in horizontal tubes: Part II-Development of a new heat transfer model for stratified-wavy, dryout and mist flow regimes," Int. J. Heat and Mass Transfer, 48, 2005b, pp. 2970-2985.

[24] J. Moreno Quiben, J.R. Thome, "Flow pattern based two-phase frictional pressure drop model for horizontal tubes. Part I: Diabatic and adiabatic experimental study," Int. J. Heat and Fluid Flow, 28, 2007a, pp. 1049-1059.

[25] J. Moreno Quiben, J.R. Thome, "Flow pattern based two-phase frictional pressure drop model for horizontal tubes. Part II: New phenomenological model, "Int. J. Heat and Fluid Flow, 28, 2007b, pp. 1060-1072.

[26] L. Wojtan, T. Ursenbacher, J.R. Thome, "Investigation of flow boiling in horizontal tubes: Part I-A new diabatic two-phase flow pattern map, Int. J. Heat and Mass Transfer, 48, 2005a, pp. 2955-2969.

[27] R.K. Shah, D.P. Seculic, "Fundamental of heat exchanger design, John Wiley & Sons Inc., New Jersey, 2003, pp. 564-574.

[28] L. Cheng, G. Ribatski, L. Wojtan, J.R. Thome," New flow boiling heat transfer model and flow pattern map for carbon dioxide evaporating inside horizontal tubes," Int. J. Heat and Mass Transfer, 49, 2006, pp. 4082-4094.

[29] L. Cheng, G. Ribatski, J. Moreno Quiben, J.R. Thome, 2008, New prediction methods for CO2 evaporation inside tubes: Part I - A two-phase flow pattern map and a flow pattern based phenomenological model for two-phase flow frictional pressure drops," Int. J. Heat and Mass Transfer, 51, 2008, pp. 111-124.

[30] L. Cheng, G. Ribatski, J.R. Thome, "New prediction methods for CO2 evaporation inside tubes: Part II -An updated general flow boiling heat transfer model based on flow patterns," Int. J. Heat and Mass Transfer, 51, 2008, pp.125-135.

[31] N.H. Kim, B. Youn, R.L. Webb, "Air side heat transfer and friction correlations for plain fin and tube HX with staggered tube arrangements, J. Heat Transfer Transactions of the ASME, 1999, pp. 662-667.

[32] SRC, "Refrigerant evaporator (DX) coil," 2001, available from: http://www.srcoils.com/File/PDF/Evap%20Coil%20Primer.pdf

Journal of Applied Mechanical Engineering and Green Technology

Journal homepage: http://ojs.pnb.ac.id/index.php/JAMETECH
p-ISSN: 2655-9145; e-ISSN: 0000-0000

Effects of temperature improvement rate on the results of coffee seeds in a coffee roasting machine with internal warming system

I.G.N. Suta Waisnawa[a1], I.M. Sudana [a], and I.M. Rajendra[a]

[a]*Mechanical Engineering Department, Politeknik Negeri Bali, Campus Street Bukit Jimbaran, Kuta Selatan, Bali 80364, Indonesia*

Abstract

The technology used to make coffee in Bangli Regency, which is a means that varies greatly from traditional to modern. Technology which is one of the same goals that is producing quality coffee. To get good quality coffee is the roasting process. The coffee roaster machine in coffee is mostly using an external heating system that is heating from outside the cylinder. Coffee or roasting time becomes less efficient because much heat is wasted. This study covers the development of coffee roaster machines with an internal heating system that uses heating elements in the cylinder, to regulate the temperature using digital thermocouples that can be adjusted according to need. The results of the test of the coffee component on the degree of light maturity result in a test value of taste above 80 which means that it is included in a special category. The productivity of the external heating system roasting is 0.41% and the internal heating system of 0.67% means that there is a difference of 0.26%. And an internal heating system that provides electricity with a usage time of 1.25 hours of Rp. 285,239 /month.

Keywords: Coffee roaster machine; internal heater; temperature improvement; productivity; product quality

1. Introduction

Coffee production in Bangli Regency, with Arabica coffee, has a unique aroma and has been accepted in international markets such as Japan, the United States, the Netherlands and France. Unfortunately, most of the coffee exported is still in the form of processed coffee (rice coffee) [1]. It is a challenge for farmers and the district government to increase the selling value of coffee production through further processing into roasted coffee or ground coffee which is currently advanced processed coffee, only able to penetrate traditional markets. In the roasting process the coffee beans will experience two important process stages, namely evaporation of water at temperatures below 160 °C and roasting at higher temperatures up to 225 °C. At a temperature of 180 °C – 225 °C the pyrolysis process occurs, the coffee will experience chemical changes such as the authoring of crude fiber, the formation of volatile compounds, the evaporation of acidic substances, and the formation of coffee-scented substances [2].

The results of a survey conducted in several coffee production centers in Bangli Regency found problems that severely hampered the production process of roasted coffee or ground coffee, namely at the stage of roasting coffee into coffee which is ready to be ground. While this stage is the stage that most determines the aroma and taste of coffee [3]. As a result, production is relatively low and of poor quality. The cause of the emergence of these problems is the use of a roaster that is not equipped with a temperature and time regulator. To ensure consistency in the quality of roasted products and the quality demands of ground coffee by consumers, the use of this machine has problems that are sufficient to hamper the production process. The machine operator must have a keen sense of smell and a high taste for the aroma of the roasted coffee. Just a little negligence causes the coffee to be scorched and of poor quality [4].

Another obstacle found in the use of this machine is the use of external heaters from gas fuel. This type of heating system is widely applied to roasting machines currently available. The external heating system, which is good heating with gas and heater, is given from outside the roasting cylinder. This system has a disadvantage that is the difficulty of controlling the temperature so that overheating often occurs due to direct contact between coffee and a cylinder plate which causes the coffee beans to burn and can reduce the quality of coffee produced. In addition, gas supply must be guaranteed to maintain the stability of the process and also the effects of gas odor that can contaminate the aroma of coffee.

[1]Corresponding author. Tel.: +628123614650; Fax: +62361702811
E-mail address: sutawaisnawa@pnb.ac.id

Roasting presents an important process step. The influence of roasting on coffee bean and cup quality was put in research focus only since several years. In our work, we were focusing on the influence of the roasting process on changes of microstructure and on the mechanisms involved in volume expansion. In the work of Geiger (2004), the influence of structure resistance forces and driving forces on volume expansion was studied in detail. Dynamic mechanical thermal analysis DMTA was applied for the identification of transition phenomena of polymeric cell wall compounds. With DMTA texture modifications such as 452 softening and hardening of materials can be identified and related to the changes of the physical state of materials. For the analysis coffee beans of different moisture content were cross-sectioned to slices of3mm thickness and mounted on a DMTA Solids Analyzer RSA II with plate-plate configuration. Then, the specimens were heated linearly from 30°C to 250°C with a heating rate of 5°C/min. Therein, the storage modulus G' is shown. The fast drop of storage modulus G' between 130 and 170°C represents a transition of polymers from the glassy to the rubbery state, the coffee bean texture is softening. The storage modulus G' increase between 200 and 230°C represents the reversion of the transition, interrupted by a melting phenomenon of a compound between 212 and 217°C. The coffee bean texture is hardening again [6].

DMTA-thermogram of a coffee bean. There is a strong relationship between initial moisture content and the temperature range of the glass transition. Because DMTA analysis was performed under non-moisture-controlled conditions, the moisture content as determined immediately at the beginning of the transition was taken into account. By variation of the initial moisture content a state diagram for coffee beans was developed. Because no sharp and pronounced transition was found in DMTA, the on- and offset of the transition was used to describe the state transition. In order to identify the compounds involved in the state modifications in green coffee beans an adapted DMTA method was applied to analyze the behavior of pure amorphous or semi-crystalline polymers prevailing in coffee bean cell walls, namely cellulose, arabinogalactan and mannan. The observed state diagram of coffee beans correlates to cellulose and mannan, whereas arabinogalactan melted completely above 210°C. Probably, the melting phenomenon observed in DMTA analysis was caused by arabinogalactan. Finally, a mixture of cell wall compounds representing the approximate composition of coffee beans was analyzed [7].

2. Methods

This research is a type of experimental research through testing prototypes of internal heating roaster machines. The roasted coffee is tested for moisture and moisture in the laboratory. Besides testing the roasted coffee from the color side using a comparison chart, and the taste or aroma of coffee was tested by a coffee tester (panelist). The parameters studied include temperature or temperature and roast time to the aroma, taste, and level of coffee dryness.

The tests conducted include: (a) Testing the productivity of the machine to determine the ability of the roaster machine with an internal heating system; (b) Testing Water Content, that is to find out the water content in certain coffee beans; (c) Organoleptic Test or Test Cup which is a quality assessment system for commodities that uses human sensory instruments as measuring instruments, such as the hands, tongue, nose, ears and eyes. People who conduct organoleptic tests are called panelists. Test results data are analyzed using the statistical program.

3. Results and Discussion

3.1 Prototype of Internal Heating Roaster Machine

This roasting process is a process where heating is carried out directly from the coffee cylinder, where the heater (heater) will immediately heat the coffee without passing through other materials so that the coffee will get even heat. But in this process it has a disadvantage where the heater used can only be an electric heater. The following is a schematic picture of the difference in the external heating process by heating in as shown in Figure 1

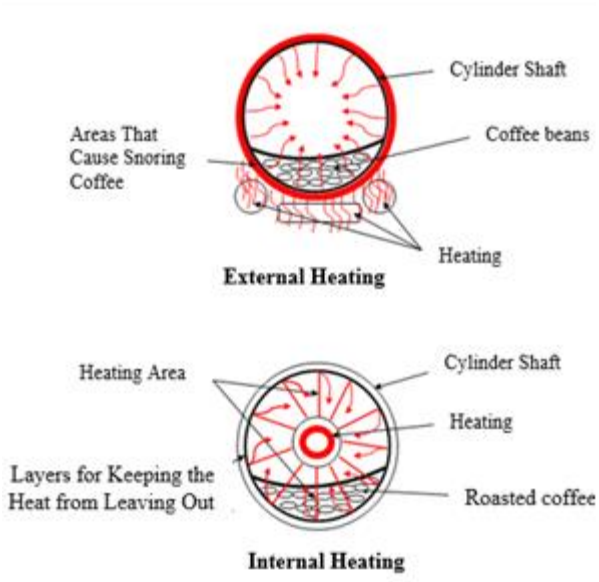

Figure 1. Differences in concepts between external and internal heating systems [5]

The results that have been achieved in this study are in the form of component design and roasting machine construction, which includes component images and dimensions, overall machine construction drawings. The design and determination of the dimensions and ingredients of the roasting machine are carried out by considering product cleanliness, energy consumption, operator safety and ease of operation and maintenance. The design process uses the Autodesk Inventor 2015 program. The roasted machine construction design can be seen in Figure 2.

3.2 Roast Machine performance testing

The test includes the function of the machine without load which consists of: the cylinder rotation mechanism, ignition system, control function of the control panel, cylinder rotation in accordance with operational modes and temperature settings. No-load machine functions can be known by visually observing all components tested after the engine is run by not directly burdening with roasting. From the results of the observation, all machine components are functioning properly. The drive and transmission motors are easily turned on and can quickly reach a stable rotation. The

roasted cylinder rotation is obtained by 13 rpm in accordance with the final design. Likewise, the internal heating system using heating elements can be operated properly [6], [7]. Setting the heating settings on the digital display settings.

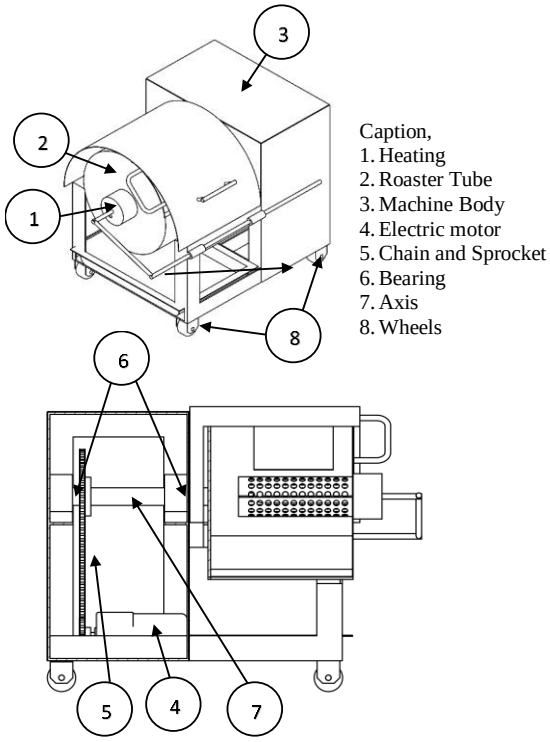

Figure 2. Design of 3D construction of coffee roasting machines through the Autodesk Inventor program

Testing the performance of roasted machines with loads carried out through the roasting process directly on the appliance. The parameters measured and the instruments used can be seen in Figure 3. Tests are carried out in stages, and repeated with the same roasting load until the total production time, relationship of roasting time, heating settings and temperature to the quality of roasted coffee are obtained for each equal load. Data retrieval in this test is done every 5-10 minutes from the beginning until the coffee is almost burnt. Part of the testing process is presented in Figure 3, while the test data is presented in graphical form in Figure 4.

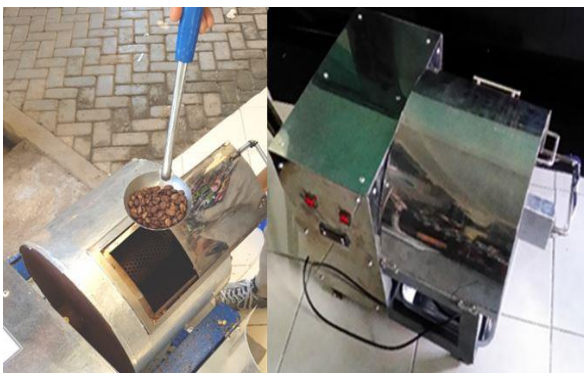

Figure 3. Roasted processes and measurement of coffee blend

Comparison of heating time in the roasting process is done by heating the coffee from outside the cylinder, where the heater in this case the heater or gas is on the outside of the cylinder wall. The heat transfer that occurs is the convection of outside air into the outer wall of the cylinder then conduction passes through the cylinder plate and finally convection from the inner wall to the surface of the coffee bean. The system requires more complicated procedures and controls, as well as more energy use, namely electricity and gas. While the internal heating system is carried out directly from the coffee cylinder, where the heater (heater) will immediately heat the coffee without passing through other materials so that the coffee will get even heat. But in this process it has a disadvantage where the heater used can only be an electric heater (heater) [8], [9]. Results Testing the rate of heat increase in the cylinder tube is the ratio of heating time as in Figure 4.

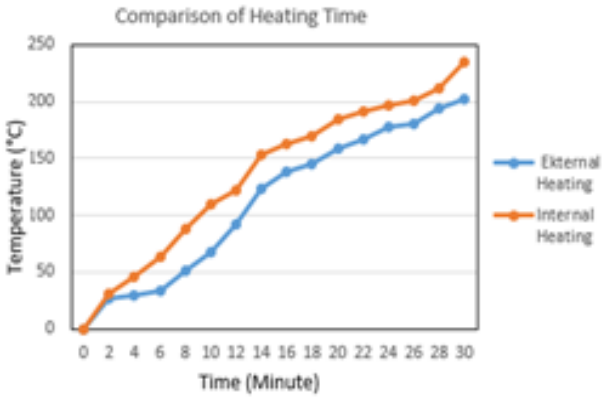

Figure 4. Comparison of time of external heating and internal heating

Machine productivity testing to determine the ability of roasting machines with an internal heating system. The following is a diagram of the temperature rise that occurs when the machine is working. As in Figure 5,

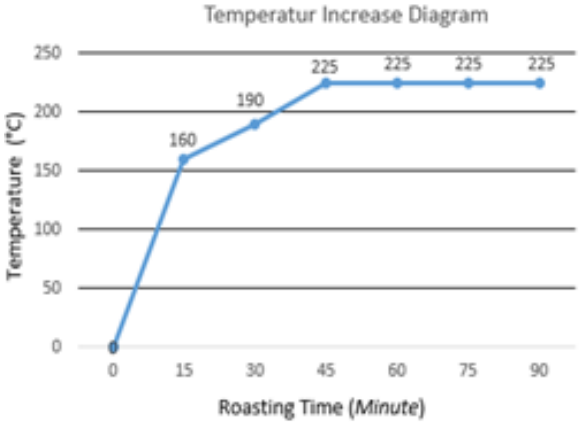

Figure 5. Temperature increase diagram

It can be concluded that it takes 15 minutes for the engine to reach a temperature of 160 ° C where at this temperature the coffee has passed the evaporation phase of the water. further testing can be conducted starting from 30 minutes, 45 minutes, 60 minutes, 75 minutes, up to 90 minutes. The test results from the coffee roaster machine,

the most appropriate time to use is roasting for 75 minutes or equal to 60 minutes after a temperature of 160 °C. The color texture of the coffee beans after heating on the roasting machine with an internal heating system as shown in Figure 6.

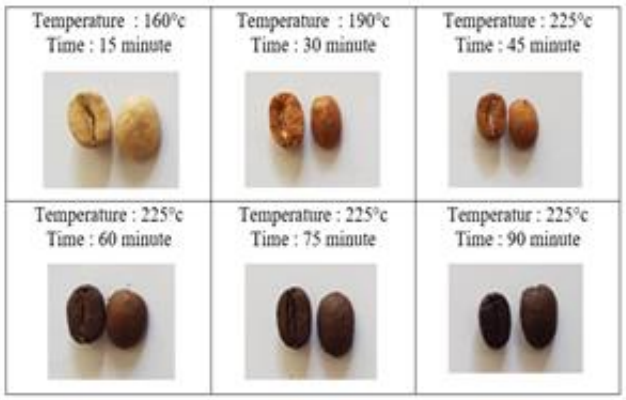

Figure 6. Texture result for Arabica coffee testing

During the roasting process takes place there is heat transfer from the heater tube (roasting media) to the material and also the mass transfer of water. The heat that causes changes in the water mass of the material due to the latent heat of evaporation [10]. This change in water mass occurs when the water content in the material has reached saturated conditions, causing the water contained in the material to change from the liquid phase to steam. Water content testing was carried out on coffee roasters for external heating systems with an internal heating system with the same loading and Arabica coffee type from the Kintamani coffee plantation in Bangli Regency, as shown in Figure 7**.**

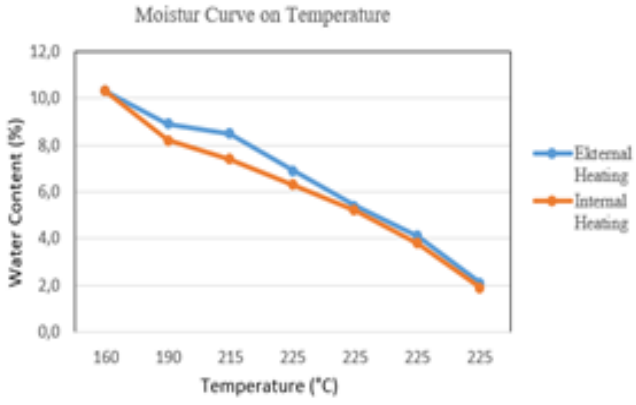

Figure 7. Moisture curve on temperature

Based on the curve of changes in coffee water content to temperature it is seen that the coffee water content will decrease with increasing roasting time. Organoleptic Test or Test Cup, a quality assessment system for commodities that uses the human sensory instruments as a measuring tool, such as the hands, tongue, nose, ears and eyes. People who conduct organoleptic tests are called panellists. The panellist acts as a measuring tool (cupper) covering sensitivity to recognize, differentiate and compare. Coffee roasting results after an assessment by the Investigator in Figure 8.

Figure 8. Results of Arabica Coffee Roast

Table 1. Results of Arabica Coffee Roasting Test

Testing Time	Test result		
	Enjoy	No favors	Uneven (%)
30 Minute	0%	100%	0%
45 Minute	0%	100%	0%
60 Minute	60%	40%	5%
75 Minute	**80%**	20%	15%
90 Minute	50%	50%	20%

From the test results obtained from the coffee roaster internal heating system, the most appropriate time to use is roasting for 75 minutes or equal to 60 minutes after a temperature of 160 °C.

Calculation of productivity is based on the process of roasting coffee because heating elements greatly affect roasting time [11]. Productivity uses external heating methods:

$$P = \frac{Output}{Input \cdot time} \times 100\%$$

$$P = \frac{0,5}{1 \cdot 120} \times 100\%$$

$$P = 0,41\%$$

Productivity uses internal heating roasting machines

$$P = \frac{Output}{Input \cdot time} \times 100\%$$

$$P = \frac{0,5}{1 \cdot 75} \times 100\%$$

$$P = 0,67\%$$

Based on the above calculations it is known that there is an increase in productivity from 0.41% to 0.67%. So it can be said that the coffee roasting machine for internal heating can increase the productivity of home industry coffee farmer producers by 0.26%.

Based on economic considerations, the roasting system of the internal heating system can increase the productivity of Arabica coffee farmers in terms of operating costs, calculation of consumption of electricity consumption in roasted machines,

The price of electricity per kWh = Rp. 1467.28 / kWh
Engine power = 540 watts = 0.54 kW
Operating time = 75 minutes = 1.25 hours
So that the costs incurred in a single machine:
Cost = engine power x operating time x electricity price
= 0.54 kW x 1.25 hours x 1467.28 / kWh
= Rp. 990,414

If calculated within a month, then:
Monthly fee =(12 hour/1.25hour x Rp 990,414) x 30 day
Monthly fee = Rp. 285,239,232 / month

4. Conclusions

The coffee roaster internal heating system results from the development of this study shows that this type of machine is able to provide a solution to the problems faced by small industries of Arabica coffee processing in increasing productivity and maintaining the quality of powdered coffee production. This roasting machine can also be operated and maintained easily, cleaner and can save production costs of more than 26% compared to an external heating system roasting machine.

Although this roasting machine has many advantages over previous roaster machines, this machine still needs to be refined and further developed in certain parts that can improve engine performance. One component that needs to be improved is the temperature control system and the heat-dampening system from the cylinder tube. Further studies on this roaster cylinder need to be done so that a more efficient roaster machine can be obtained with components that can be made entirely (locally) and at affordable prices for coffee farmers or small industries.

References

[1] BPS, ”Bali dalam angka 2017,” 2017, Denpasar: BPS Propinsi Bali.

[2] D. Bottazzi, S. Farina, M. Milani, and L.Montorsi, ” A numerical approach for the analysis of the coffee roasting process, ” Journal of Food Engineering, 112, 2012, pp. 243–252.

[3] J. Baggenstoss, L. Poisson, R. Luethi, R. Perren, and F. Escher, ”Influence of water quench cooling on degassing and aroma stability of roasted coffee,” Journal of Agricultural and Food Chemistry, 55, 2007, pp. 6685–6691.

[4] P. Bhre, “Metode Sangrai Kopi”, 2017, http:// kopitravel.blogspot.co.id, diunduh pada tgl 27 Pebruari 2018.

[5] A. Fabbria, C. Cevolia, S. Romanib, M.D. Rosab, ”Numerical model of heat and mass transfer during roasting coffee using 3D digitised geometry,” Procedia Food Science, 1, 2011, pp. 742-746.

[6] C.T. Gayo, ”Standar Umum Pengujian Mutu Pada Biji Kopi”, 2017, www.tpsaproject.com diunduh pada tanggal 28 Pebruari 2018.

[7] R. Geiger, “Development of coffee bean structure during roasting – Investigations onresistance and driving forces”, 2004, [DPhil thesis]. Zurich, Switzerland: Swiss FederalInstitute of Technology (ETH); Number 15430.

[8] R. Geiger, R. Perren, R. Kuenzli, F. Escher, “Carbon dioxide evolution and moistureevaporation during roasting of coffee beans”, Journal of Food Science, 2004 (in press).

[9] J.A. Hernández, B. Heyd, G. Trystram, ” Prediction of brightness and surface area kinetics during coffee roasting,” Journal of Food Engineering, 89, 2008, pp. 156-163.

[10] P. Lestari, “Teknologi Pengolahan Kopi”, Kementeri-an Pertanian Badan Penyuluhan dan Pengembangan SDM, 2016, Balai Penyuluhan Pertanian Jambi.

[11] S. Najiyati, dan Danarti, ”Kopi, Budidaya dan Penanganan Lepas Panen,” 1990, Edisi I, Jakarta: Penebar Swadaya.

[12] I.M. Rajendra, I.N. Suamir dan I.G.N. Suta Waisnawa, “Pengembangan dan optimasi mesin sangrai kopi yang hemat energi untuk meningkatkan kualitas produksi” Proceding Senapati Technopreneurshif, 2013, Politeknik Negeri Bali

[13] S. Schenker, C. Heinemann, M. Huber, R. Pompizzi, R. Perren, F. Escher, ”Impact of roasting conditions on the formation of aroma compounds in coffee beans,” Journal of Food Science, 67, 1999, pp. 60-66.

[14] S. Schenker, “Investigations on the hot air roasting of coffee beans” 2000, [DPhil thesis].Zurich, Switzerland: Swiss Federal Institute of Technology (ETH); Number 13620.

[15] S. Schenker, S. Handschin, B. Frey, R. Perren, F. Escher, “Pore structure of coffee beansaffected by roasting conditions”, J Food Sci 65, 2000,, pp. 452-57.

Journal of Applied Mechanical Engineering and Green Technology

Journal homepage: http://ojs.pnb.ac.id/index.php/JAMETECH
p-ISSN: 2655-9145; e-ISSN: 0000-0000

Possibility analyses of using hydrocarbon R-290 and mixing with R-32 refrigerant to retrofit R-32 domestic split air conditioning

M.E. Arsana[a1], I.D.M.C. Santosa[a], I.B.G. Widiantara[a], and I.W. Temaja[a]

[a]*Mechanical Engineering Department, Politeknik Negeri Bali, Badung, Bali 80364, Indonesia*

Abstract

Indonesia government's policy to eliminate the use of R-22 refrigerant in air conditioning cooling system will be enforced by 2020. Air cooling equipment manufacturers, especially domestic air conditioners, dominate Indonesia and Asia markets using R-410a and R-32 refrigerants as a replacement to R-22. This study will present the results of experimental studies of retrofit testing on the system of split type domestic AC using R-32 with hydrocarbon refrigerant and Mixing with R-32. The use of hydrocarbons as a refrigerant retrofit is very potential to retrofit R-32 in split type domestic AC without replacement of any part of the system provided that its possibility study has been performed through theoretical and experimental study. An analysis is also done to provide the solution for split AC utilization using R-32 refrigerant retrofitted with hydrocarbon refrigerant. Testing has been done by simply replacing the refrigerant without replacing any component. This experiment uses commonly used ½ Pk split type domestic AC equipment whose equipment consists of a semi-hermetic inverter compressor, condenser and capillary pipe expansion valve in the outdoor unit and an evaporator as a heat exchanger in the indoor unit. Results obtained in preliminary data processing showed that R-32 retrofit with HR-290 hydrocarbon refrigerant and mixing with R-32 deals with improved COP performance from 4.65 to 5.0, 5.47 respectively with reduced energy use.

Keywords: COP; refrigeration system; retrofit; refrigerant; and energy use

1. Introduction

Here one of point declared in the Montreal and Kyoto protocol (1897 & 1997) was banded the using of refrigerant R-22 (HCFC-22) and changed it by the refrigerant which friendly with environment. The alternative is hydrocarbon refrigerant but because it is flammable, the use is limited. [1]. Recent research on topics leads to HFCs and natural refrigerants such as water (R718), ammonia (R717) and CO_2 (R744) with very low ODP and GWP used to replace HCFCs in refrigeration and AC systems [2]. Manufacturers and importers of air conditioning refrigerants prefer refrigerants such as R-32 and R-410a refrigerants to be applied to air-conditioning systems. Both of these refrigerants have zero ODP and low enough GWP of 675 for R-32 and 2088 for R-410a as well as non-flammability due to its low flame nature [3].

The R-22 cooling machine can still be used by retrofit or drop in refrigerant method from R-22 to R-290 because the compressor oil used on R-22 can be used for R-290[4]. An experimental study with split AC replaced by R 290 showed that its cooling capacity decreased by 1.6% and COPR was higher by 10%. Along with the concern for the Environment the regulation for split AC with R-22 is getting tighter.

The energy efficiency labels (EEL) published in 2007 that a split-market COP with a capacity below 4.5 kW should be no less than 3.2 [5]. The researchers conducted an experimental study with R-22 retrofit small wall room air conditioner with R-290 which found that COP R-32 and cooling capacity were higher than the original but with a heat exchanger with 7 mm diameter tube which by increasing the diameter means to increase production cost also increase the amount of refrigerant inserted so that the maximum refrigerant fill in is below the security standards set for the refrigerant and also flammable. Some researchers are discussing R-32 refrigerants such as; [6] presented that the two-stage suction ejector cycle using R-32 theoretically resulted in the development of this cycle resulted in higher COP cooling and heating capacities but continued with experiments. [4].

Presenting theoretically that R-32 can be used to replace R-410 by utilizing refrigerant flow system (VRF) that R-32 COP is 5% higher and its cooling capacity is 6% results obtain based on system thermodynamic analysis it is known that R-32 COP is 5% higher and its cooling capacity is 6% higher than R-410.

[1]Corresponding author. Tel.: +6281338636816; Fax: +62361702811
E-mail address: eryarsana@pnb.ac.id

Nomenclature

E_{annual}	Energy consumption, in kW/y	n	System operating time, in year
h_{in}	Enthalpy air entering air handling unit (AHU), kJ/kg	ß	CO_2 emission, in Kg/kWh
h_{out}	Enthalpy air out AHU, kJ/kg		
$\dot{m}$	Mass flow rate air, kg/hr		

For that reason, some countries in the world provide alternatives refrigerant such us: Japan with R32, USA with R 410A, Europe with HFC, PFC, SFC, Australia with SGHG (synthetic greenhouse gases), Indonesia with R32, Basic Regulation used is International regulation [7]. Due to differences in technical specifications, especially the working pressure of refrigerant then the cooling machine using R-22 is not possible to retrofit with R 32. In Indonesia the new air conditioner has been imported from China and Japan and used R-32 The consequence is of course in terms of price more expensive because of technical specifications increased such as compressor with a larger capacity and equipped with inverter, condenser pipe with a larger diameter of 6 mm thicker and the price of refrigerant twice more expensive.

Various efforts have been made to find an alternative refrigerant to comply with environmental friendly. The concern of the Indonesia Government on ozone layer protection is stated in Presidential Decree No. 23/1992 and the decisions of ministry commerce and industry No. 110 / MPP / Kep / 1/1998 which contains restrictions on the use and production of ozone depleting substances. To be able to produce products that meet the standards, the government has formulated the Indonesian National Standard (SNI) in the field of hydrocarbons as a strategic step.

Some of the natural refrigerants already used in refrigeration machines such us ammonia (NH_3), hydrocarbons (HC), carbon dioxide (CO_2), water, and air [8]. The use of carbon dioxide, water, and air in commercial refrigerators still requires an extensive research, while the use of ammonia and hydrocarbons still considerable and has a lot of research opportunities. Ammonia is toxic and flammable, while hydrocarbons are included in highly flammable substances; therefore, the refrigerant is generally difficult to use on a direct expansion system. Indirect refrigeration system can be used to overcome the weakness of both refrigerants. Some researchers try to suppress the hydrocarbon refrigerant's level of combustion by mixing it with other non-flammable refrigerants [9]. The study aims to optimize energy use through performance improvements (COP) in air conditioning systems of water-cooled chillers.

These performance improvements are made using appropriate primary refrigerants, as well as the addition of additives to secondary water refrigerants that can provide energy saving effects maintenance approach temperature at condensers. From the result of the research, the best performance improvement was achieved in combination of R-290 primary refrigerant with 0,7 Water +0,3 Tri-methylolethane (mass base) as secondary refrigerant. In this condition the increase the cooling machine performance coefficient is about 42%, saving power consumption 30% (in compressor) and increase cooling capacity about 10%.

In Germany, the latest refrigerators using R-600a and heat pumps and air conditioners now use the R-290 with measurable energy consumption 10 to 20% lower than R-12, R-134a or R-22 [10]. By applying the drop in method using R-290 refrigerant to replace R-22. The test was performed using the Indian standard IS 1391 (1992), states that by refueling refrigerant half of R-22, the cooling capacity is lower 6% compared to R-22. The energy consumption decreased 15.4% and discharge temperature decreased 20°C. So the energy efficiency ratio (EER) is 14% higher than R-22 [11] has also conducted an experiment to replace R-22 and R-410A for mini AC split.

It also performs on 6 other refrigerants, including R290 under different environmental temperature conditions, where the outdoor temperature varies from 27.8 °C up to 55 °C. This is followed by soft optimization, which sets the capillary tube diameter, from 2.0 mm to 1.65 mm and changes the length from 508 mm to 254 mm, using the same Ac split where the result indicates that propane is the most suitable refrigerant for alternative R-22 [12] with the aim of comparing the thermal performance of refrigerants R-22, R-290, R-1270, R-438A, R-404A, R-410A and R-32 with evaporator temperatures varying from -15 °C to -5 °C, using electronic expansion valve and variable speed compressor.

Systems with R-22 refrigerant are used as the basis of comparison only by replacing refrigerant in case for oil HFCs on the system are also replaced. [13] Its environmental impact is measured by the TEWI (Total Equivalent Warming Impact) parameter. The results show that the use of R1270 and R290 gives a maximum COP value. As well as other advantages of lowering the consumption of electrical energy, reduce the use of refrigerant, low HCs and low GWP. Based on that problem, it will need technical studies and experimental testing for R-32 refrigerant retrofit with hydrocarbon refrigerant with loading in the test chamber to obtain COP and assessment for environmental impact.

2. Methods

This research method will be done by drop in method [14] when these methods allow replacing R-32 refrigerant with R-290 and R-290 mixing R-32. Without replacing its components. The test will be use split air-conditioning domestic 1 Pk which is common in Indonesia market. Major parameters such as temperature and pressure on the system are used to verify and calculate performance. The comparison between the three refrigerants will use the same AC with the help of the ESS program [13]. The TEWI parameter is used to determine how much the impact on the environment due to the use of both refrigerants is attributed to BS EN 378, 2008 standard.

1.1 Type, Design and Place of Study

The experimental research method was implemented by direct observation, and by performing several treatments, the R-32 and R-290 refrigerants were tried alternately according to the procedure to determine the changes that occurred in the observed parameters. The data obtained by measurement will be recorded on the installed acquisition data and then intended for the calculation of the COP and EER values of the system, energy use and environmental impact assessment**.** In this study designed included some activities i.e. preparation (literature study, field observation), tool design, retrofit, evacuation, vacuuming and leakage test of oil lubricant replacement (hydrocarbon) and running test. This test will be conduct at Laboratory of Refrigeration and air Conditioning Study Program Department of Mechanical Engineering, Bali State Polytechnic.

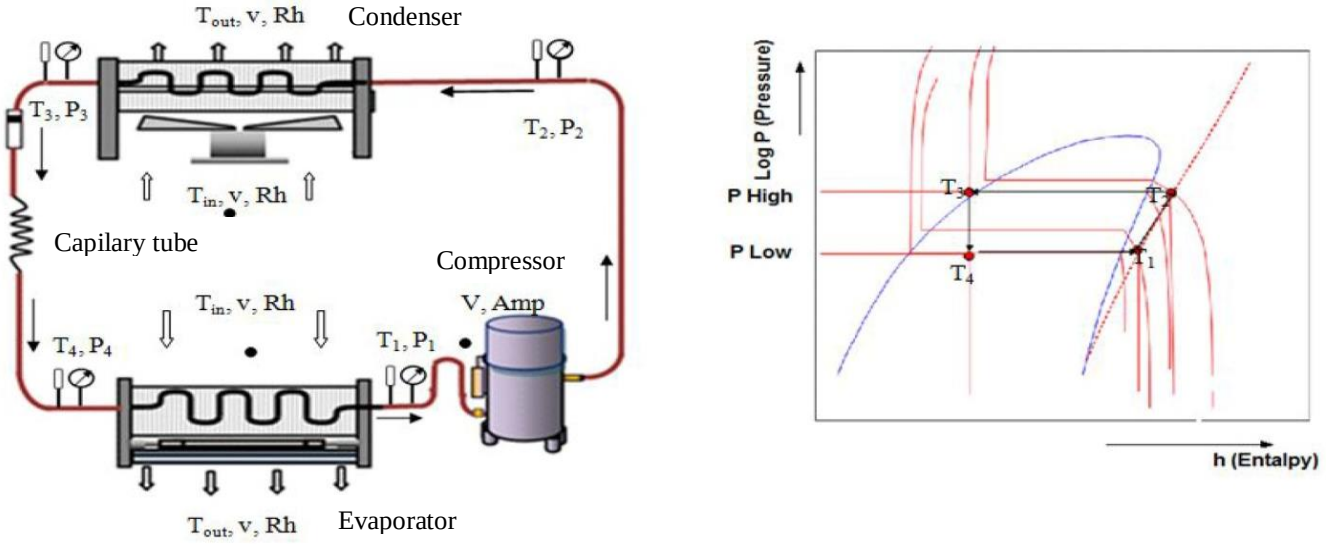

Figure 1. The vapor compression cycle

1.2 Procedure

The test research procedure is carried out in a room with good insulation, following the AHRI 210/240 Standard with load variations from 0.5, 1, 1.5, 2, to 2.5 kW using an electric heater. See Figure 1. Data obtained from this research is primary data. All instruments, including gauges and thermometers, will be calibrated during the measurement test range. The data will be taken on the evaporator and compressor with the following parameters:

Evaporator:

a. Dry air temperature and mass flow rate entering evaporator
b. Temperature out at coil evaporator
c. Relative air humidity in and out evaporator

Compressor:

a. Energy consumption comp
   The data is taken every 10 minutes, a single test take 3 hours. The test will be conducted 3 times the analysis, the data will be averaged first.

1.1 Preparing the measurement

The following standard procedure used in determining AC performance [17] will be used on psychometric charts to determine enthalpy (heat content in inlets and outlets)

$$Heat\ Load\ (TR) = \frac{\dot{m}\ (hin - hout)}{4.18\ x\ 3024} \quad (1)$$

The heat load can be calculated theoretically by estimating the sensible heat load and latent heat in the air-conditioned room. The difference between the two shows losses due to leaks, unwanted loads, etc.

1.3 Method of Measurements

a. The rate of air mass flow is calculated by finding the flow velocity of the inlet air as well as determining the extent of the inlet side air in the split air
b. The amount of enthalpy is obtained from the psychometric chart by measuring the temperature and Rh at the air inlet and outside of the evaporator coil (indoor unit)
c. The energy consumption by compressor can be measured with a portable power analysis tool that will provide direct reading in kW. If not present, the ampere shall be measured with an available on-line ohm meter or by using a tang tester. The power can then be calculated assuming a power factor of 0.9 by the formula.

$$\text{Power (kW)} = \sqrt{3}\ \text{xVx I x cos}\ \emptyset (2)$$

Performance calculations can be used values as shown in Table 1.

Table 1. Conversion factor for refrigeration performance

COP = 0.293 EER	EER = 3.413 COP
kW/Ton = 12 /EER	EER = 12/(kw/Ton)
kW/Ton = 3.516 /COP	COP = 3.516/kW/Ton

Source: *American refrigeration institute*

d. The TEWI parameter is used to determine how much the impact on the environment due to the use of all refrigerants is attributed to BS EN 378, 2008 standard. TEWI assessment (total equivalent warming impact) by assuming losses of leakage and recovery ~ 0 can be calculated using the TEWI formula approach only is the impact of energy consumption:

$$TEWI = n \times Eannual \times ß \quad (3)$$

Figure 2. Instrumentation of the test system

3. Results and Discussion

From the data that has been obtained in the measurement as shown in the picture below will be followed by using MS-Excel program. The results obtained by EES program will then be plotted on the P-h diagram to get its COP value.

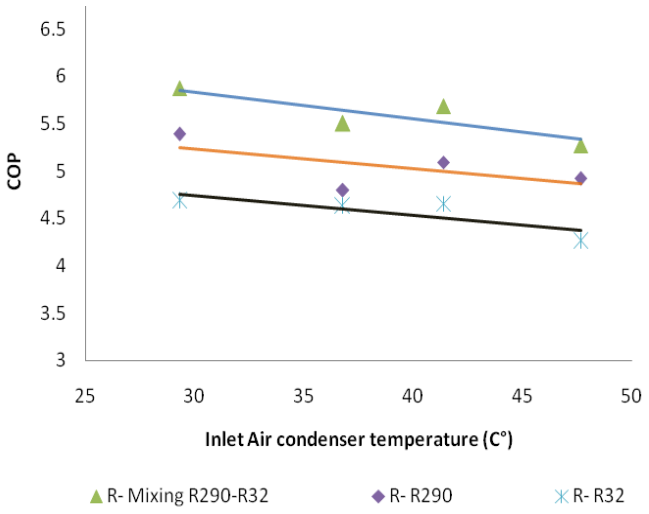

Figure 3. COP system

Another result is the comparison between the Inlet Air condenser temperature with the power compressor used by the compressor and the ratio of condenser and evaporator temperature.

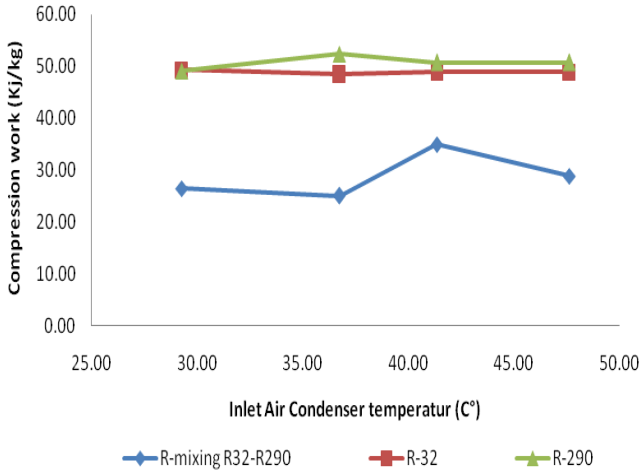

Figure 4. Compression work

From pictures above, Figure 3 we can see some different COP the highest COP value of 5.47 was Refrigerant mixing R-290/R-32 and then R-290 with average COP 5.0 and the R-32 COP refrigerant is 4.65. For mixing R290-R32 refrigerant are obtained by using the R410a refrigerant properties. Comparison of the compression works in kJ / kg sees Figure 4. The red line is for R-32 refrigerant while the green color is R-290 refrigerant and blue is the mixed refrigerant. From the comparison of the compression work, it is known that mixed refrigerants have the smallest compression work so that the use of electricity is reduced by an average compression work for the use of mixed refrigerants of 25.78 kJ / kg. When compared with compression work for R-32, the average value is 48.89 kJ / kg then there is a decrease in power usage by 0.47.

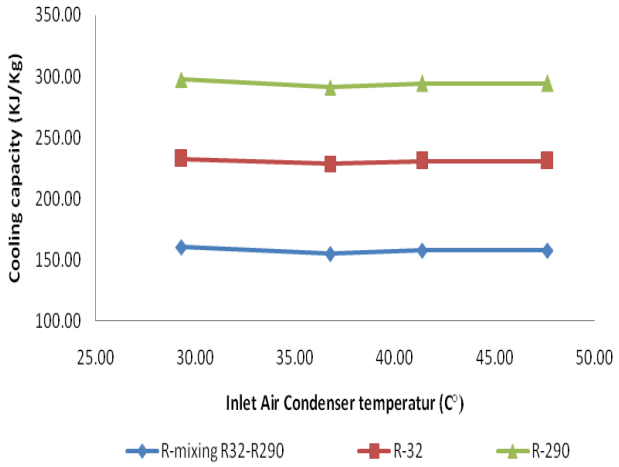

Figure 5. Cooling capacity

Figure 5 shows the comparison of its cooling capacity. The highest cooling capacity is R-290. The mixed refrigerants it has the smallest cooling capacity as a result of a decrease in its compression work. It can also be said to be the result of mixing R-32/R-290 refrigerants so that they have their own performance characteristics. The evaporator temperature of the mixed refrigerant is an average value of 19.46 °C so that it is higher than the refrigerant R.32 whose value is 12.88 °C.

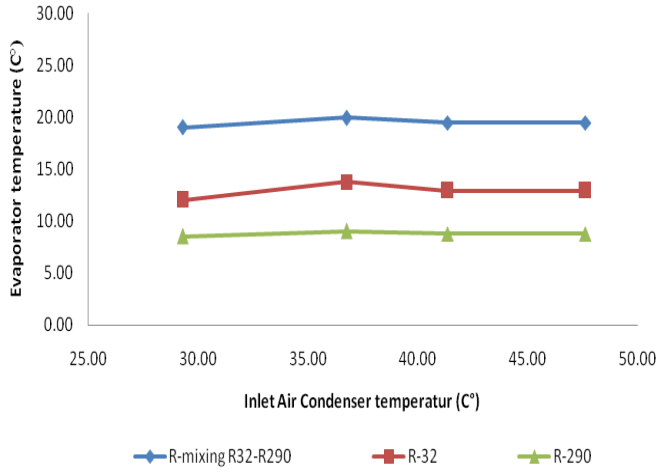

Figure 6. Evaporator temperature

Achievements for the R-290 have the lowest average value of 8.75 °C among them. this indicates that the temperature performance is best achieved by retrofit it with R-290.

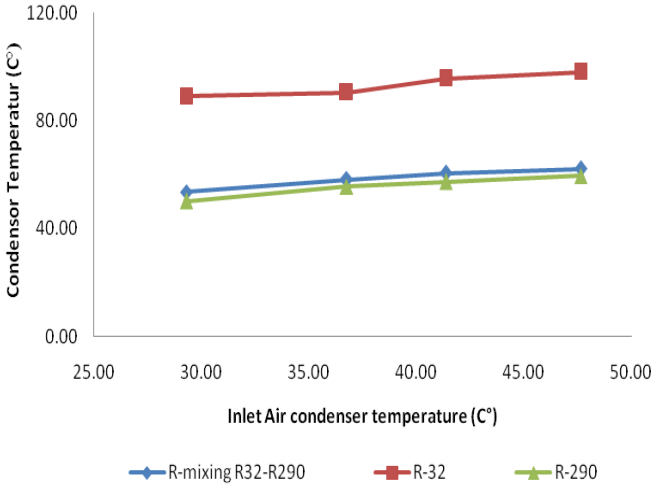

Figure 7. Condenser temperature

Figure 7 shows temperature of the condenser measured on the discharge side is based on the measurement results that the discharge temperature of refrigerant R-32 for the condenser inlet air temperature is 29.5 °C is 89 °C. while the use of a mixture of R-290/R-32 refrigerants approached the discharge temperature of R-290, respectively 58.60 ° C and 50.76 °C. In Figure 8. shows the power used by the compressor. The highest value is indicated by the use of the refrigerant R-32 which is 5.08 kWh, then the R-290 is 3.83 kWh and the lowest is the R mix R32-R290 with an average value of 3.02 kWh so there is a potential energy savings of 39% for refrigerant mixture R-32/R-290 and 25% for the use of refrigerant R-290. While the impact on TEWI system, which is a way to assess global warming by combining direct contributions from refrigerant emissions the air conditioning, split system is 0.5 Pk. See Figure 9. TEWI value for Refrigerant R-32 is 1339.74 Kg eq.CO_2 per year and for R-290 is 964,241 Kg eq.CO_2 per year while the lowest is for Mixing R-32/R-290 refrigerant.

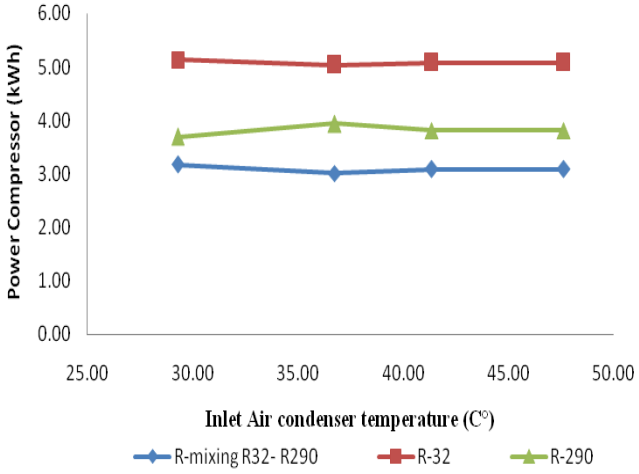

Figure 8. Power of compressor (kWh)

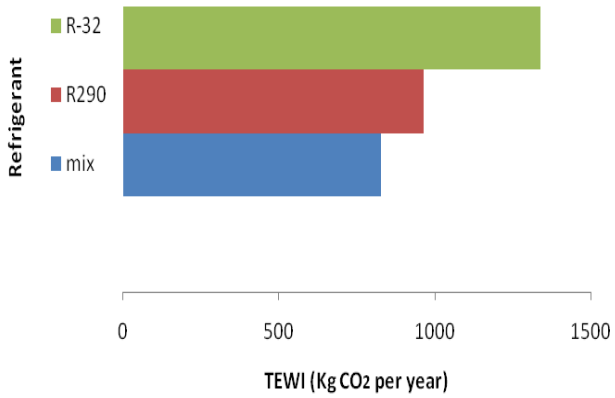

Figure 9. TEWI total equivalent warming impact

This is 828.52 Kg eq.CO2 per year. Thus, there is an opportunity to reduce its environmental impact for refrigerant R-290 and mixing the R-32/R-290 by 28%, 38% respectively

4. Conclusion

The possibility to use R-290 and mixing R-32 / R-290 to retrofit R-32 without replacement equipment is possible. From the research, we can see some primary parameters, which are indicated by R-290 having similar characteristics with R-32 but with some advantages as well as if they were mixed based on the composition of 40:60 for R-290 and R-32. COP improvement 15% for R-290 and 25% for R mix R32 / R290. Potentials energy saving at the compressor is 39% for refrigerant mixture R-32/R-290 and 25% if replaced with Refrigerants R290. TEWI has a reduction potential of 28% to 38%.

Acknowledgments

The authors acknowledge the financial support received from the Higher Education Directorate General of the Ministry of Research, Technology and Higher Education of the Republic of Indonesia.

References

[1] M.Y. Taib, A.A. Aziz, and A.B.S. Alias, "Performance Analysis of a Domestic Air conditioner," National Conference in Mechanical Engineering Research and Postgraduate students, 2010.

[2] M. Mohanraj, S. Jayaraj, and C. Muraleedharan, "Environment friendly alternatives to halogenated refrigerants - a review", International Journal of Greenhouse Gas Control 3, 2009, pp. 108–119.

[3] C. Yıldırım, D.B. Özkan, and C. Onan, "Theoretical study of R-32 to replace R-410A in variable refrigerant flow systems". International Journal of Ambient Energy, 2017.

[4] E. Granryd, "Hydrocarbons as refrigerants e an overview", Int. J. Refrig. 24, 2001, pp.15-24.

[5] J.H. Wu, L.D. Yang, and J. Hou,." Experimental performance study of a small wall room air conditioner retrofitted with R-290 and R-1270", Int. J. Refrig. 35, 2012, pp. 1860-1868.

[6] J.L. Yu, X. Song, M. Ma, "Theoretical study on a novel R-32 refrigeration cycle with a two-stage suction ejector", Int. J. Refrig. 36, 2013, pp. 166-172.

[7] Ashrae Handbook, "Fundamentals American Society of Heating, Refrigeration and Air Conditioning Engineers". 2005 SI Edition.

[8] M.O. McLinden, J.S. Brown, R. Brignoli, A.F. Kazakov, and P.A. Domanski, "Limited options for low-global-warming-potential refrigerants". Nature Communications, 2017, www.nature.com/ naturecommunications

[9] I.N. Suamir, I.N.G. Baliarta, M.E. Arsana, and I.W. Temaja, "The Role of Condenser Approach Temperature on Energy Conservation of Water Cooled Chiller," Advanced Science Letters, 23, 2017, pp. 12202-05.

[10] A.S. Padalkar, K.V. Mali, and S. Devotta, "Simulated and experimental performance of split packaged air conditioner using refrigerant HC-290 as a substitute for HCFC-22". Applied Thermal Engineering, Volume 62, 2014, pp. 277-284.

[11] O. Abdelaziz, S. Shrestha, J. Munk, R. Linkous, W. Goetzler, M. Guernsey, and T. Kassuga, "Alternative Refrigerant Evaluation for High-Ambient-Temperature Environments: R-22 and R-410A Alternatives for Mini-Split Air Conditioners", Report: ORNL/TM-2015/536, 2015, Oak Ridge National Laboratory, USA,

[12] A.H.P. Antunes, and E.P.B. Filho, "Experimental investigation on the performance and global environmental impact of a refrigeration system retrofitted with alternative refrigerants International ". Journal of Refrigeration, 16, 2016, pp. 1-8.

[13] BSI Standards Publication, Refrigerating systems and heat pump safety and invironmental equipment, The British standards institution, 2016. Methods of calculating total equivalent warming impact (TEWI) ISBN 978 0 580 84660 1.

[14] H. Pham, and R. Rajendran, "R-32 And HFOs As Low-GWP Refrigerants For Air Conditioning", Emerson Climate Technologies Inc. Sidney, Ohio 45414 USA. International Refrigeration and Air Conditioning Conference at Purdue, 2012, 2262, July 16-19,

[15] A.S. Padalkar, K.V. Mali, D.D. Rajadhyaksha, B.J. Wadia, and S. Devotta, "Performance assessment of air conditioners with HC290", in: 9th IIR Gustav Lorentzen Conference, 2010, Sydney, Australia.

[16] R.C. Jordan, and G.B. Priester "Refrigeration and Air Conditioning". Prentice Hall of India pvt.ltd.

Journal of Applied Mechanical Engineering and Green Technology

Journal homepage: http://ojs.pnb.ac.id/index.php/JAMETECH
p-ISSN: 2655-9145; e-ISSN: 0000-0000

A study on improving torsional power of carbon steel St.37 with 800 ºC heating and fresh water quick cooling

I.K. Rimpung[1]

Mechanical Engineering Department, Politeknik Negeri Bali, Campus Street Bukit Jimbaran, Kuta Selatan, Bali 80364, Indonesia

Abstract

The steel St.37 is often used as a machine component or as a shaft material, because it is relatively inexpensive and easily heat treated. Heat treatment of steel St.37 is used to get the desired strength change. It means, before being used in construction techniques, the resistance of steel to external loads as a technical material is very important to know. Due to the resistance of external loads, for example in the form of twisting on the shaft or engine components in appropriate technology is very common. The change of steel strength by the external load is carried out by heat treatment, which through the heating process to a certain temperature and the cooling process using certain media and with a certain cooling speed as well. This study examines how much the standard steel torsion strength (St.37) is increases compared to the same type of steel after going through the 800 ºC heat treatment process with rapid cooling using fresh water. The testing of this study is carried out on the Torsion Measuring Testing Machine Model N-50, together with the fourth semester students, in the material and metrology testing laboratory of the Bali State Polytechnic Mechanical Engineering Department. As a result, steel St.37 hardening through 800◦C heating and cooled quickly using fresh water, compared with standard steel (St. 37), it seen from the test results, namely: Maximum steel twist stress St.37 Standard: 503.7021855 $N.mm^{-2}$ at the maximum torsional moment is 24.6 Nm, whereas, the maximum torsional stress of St.37hardening steel: 697.8735409 $N.mm^{-2}$ at a maximum torsional moment of 35.4 Nm. The elasticity modulus (G) of each specimen after being calculated using relevant formulas, is obtained: G (St.37 standard) = 4205.500677 ($N.mm^{-2}$) G (St.37 hardening) = 1335.750379 ($N.mm^{-2}$).

Keywords: Steel; heat treatment; twist stress; twisting resistance; and hardening

1. Introduction

The Department of Mechanical Engineering, Bali State Polytechnic (PNB) directs students to design appropriate technology tools or machines before completing their study at PNB. The results of student design are expected to be more reliable and able to meet the needs of the community. Reliable machines or equipment are machines or tools in their working processes that are safe for operators and their environment, and guaranteed sustainability in their maintenance and repair, also are able to produce competitive products [1].

The choice of material to be used as a component of a machine or tool must be in accordance with the designation and mechanical properties in order to meet the criteria and the burden that occurs on it. Mechanical properties of materials or steel can be known through several testing processes in material testing laboratories. Steel is a technical material that results from advanced processing of crude iron through a smelting process in the converter consisting of the main elements metal or Ferro, carbon, manganese, phosphorus and Sulphur [2]. Heat treatment of steel is intended to obtain the desired mechanical properties, namely heating process with a certain temperature in a heating kitchen and cooled by using certain media as well [3].

This study examines the increase in St.37 steel torsional resistance which gets warmed to 800 ºC and cooled rapidly using fresh water. The choice of steel as mentioned above (St.37) is because the material is widely used and generally available on the market and meets the requirements as a raw material for tool components or machinery of appropriate technology. The hardness testing process is carried out on a specially designed machine that can provide information on the torsional strength of the test object, [4]. This research is a study to determine the extent of the increase in standard St.37 steel torsional strength compared to St.37 steel which is hardened or heat treated based on the theories of materials testing technology especially steel [2].

[1]Corresponding author. Tel.: +6285101897681; Fax: +62361702811
E-mail address: ketutrimpung@pnb.ac.id

Nomenclature

τp	Torsional tension (N.mm^{-2})	θ	Twisting angle (º)
Mp	Twisting moment (N.mm)	ϕ	Specific twisting angle (º.mm^{-1})
Wp	Moments of detention (mm^3)	l	Work piece length (mm)

The objectives of this study include: (i) To obtain torsional moment data that occurs on St.37 pavement / hardening steel; (ii) To obtain data on the value of steel torsional strength St, 37 with heat treatment; (iii) To compare the changes of the standard St.37 steel torsional angle with St.37 pavement; (iv) To know the elasticity modulus of St.37 pavement steel. The results of this study are expected to provide benefits. This research is very useful for researchers and students to develop and deepen their knowledge in the field of material technology, as well as to increase skills in the implementation and operation of materials testing tools. For Bali State Polytechnic institutions, this research is useful to introduce to the parties so that it can be used as a source and comparison of relevant research results. For the community especially those who are dealing with the design and selection of steel materials, the results of this study can be used as a guide in the removal of technical materials in the form of metals and non-metals in general and steel particularly in St.37.

2. Method

This study was carried out by collaboration of fourth semester students who conducted material test practical activities at the Material and Metrology Test Laboratory, Mechanical Engineering Department, Bali State Polytechnic. The process of this research is carried out through two stages, namely: the first stage of the formation of dimensions, by smoothing the surface and the length of the test object, including heating of the specimen in the heating kitchen until it reaches a temperature of 800 ºC, then cooled quickly using fresh water.

The second stage is the data collection on the torsion testing machine, namely; Torsion Measuring Testing Machine Model N-50. This study tested the twisting of the specimen regularly and gradually measured until the test object broken. Therefore, testing specimens directly against standard or hardened test objects [5]. Test specimens were tested for each of the five sticks on the hardness testing machine. The testing process starts from installing the test object on the stand with the torsion angle 00 and adjusting the load by twisting the work-piece through the load input by turning the hand-wheel. The reading of the torsional moment data starts from a multiple of twisting 100 until the test object breaks, and the twisting moment returns to zero. Thus the testing process is carried out by each test object five times carefully until completion [6].

Tests using the Torsion Measuring Testing Machine Model N-50 obtain primary data in the form of the magnitude of torsional angle readings and twisting moments that occur based on the research requirements. Other data needed are calculated using relevant formulas, namely:

a. The voltage drop (τp) is calculated by the formula:

$$\tau p = \frac{Mp}{Wp} \left(\frac{\mathrm{N}}{\mathrm{mm}}\right) \quad (1)$$

Wherein:
Mp = Moments of twisting that occur (N.mm)
Wp = Torsion resistance that occurs (mm^3)

For solid and round sections:

$$\mathrm{Wp} = \frac{\pi d^3}{16} . \quad \text{.. .(2)}$$

Wherein:
d = diameter of the test object (mm).

b. The twist angle is divided by the length of the work piece (l), then a specific twisting angle is obtained:

$$\theta = \frac{\phi}{l} \left(^{\circ}.mm^{-1}\right) \quad (3)$$

Furthermore, the torsional moment-twist angle diagram and the specific torsional stress angle diagram (*shearing stress-specific angle of the twist diagram*) can be described based on the data obtained directly from the torsion testing machine and data calculated based on the formulas [7].

c. In the same situation, the moment of polar inertia can be calculated or worked through the shear or twist torsion modulus. By giving a torsional moment a shear stiffness modulus (G) is obtained or also called a shear modulus. Within the proportional limit, the following formula can be calculated as follows.

$$\phi = \frac{Mp.l}{G.lp} \left(radian\right) \quad (4)$$

$$= \frac{Mp.l}{Gp.Ip} \frac{360^{\circ}}{2\pi} \left(^{\circ}\right) \quad (5)$$

Wherein:
ϕ = twisting angle $(^{\circ})$
Mp = the twisting moment happened (N.mm)
l = work piece length (mm)
Ip = moment of polar inertia (mm^4)
G = tension or shear modulus (N.mm^{-2})

For solid and round sections:

$$Ip = \frac{\pi r^2}{2} \quad \text{or} \quad \frac{\pi d^4}{32} \quad (6)$$

3. Results and Discussion

3.1 Test Results

This research has been carried out with students of the Mechanical Engineering Department, Bali State Polytechnic, batch 2011/2012, it was carried out meticulously and systematically under the supervision of researchers, starting from testing St.37 standard specimens and St.37 hardening. The test results carried out by each type of test object as much fifteen times, noted and processed with the appropriate formulas and then entered into Table 1 which shown Test I (St.37 Standard) of diameter x Length: 6.29 mm x 31.27 mm and Table 2 shows Test II (St..37 Hardening) diameter x length: 6.37 mm x 30.48 mm.

Table 1. Steel St.37 Standard Test Data

Reading angle (°)	Torque (N.m)	Tension Voltage ($N.mm^{-2}$)	Specific Tapping Angle ($°.mm^{-1}$)
10	1.6	32.76111775	0.319795331
20	22.4	458.6556486	0.639590662
30	24.6	503.7021855	0.959385993
40	22.7	464.7983581	1.279181324
50	18.7	382.8955638	1.598976655
60	8.3	169.9482983	1.918771986
70	5.3	108.5212026	2.238567317
80	1.3	26.61840818	2.558362648
90	0.6	12.28541916	2.878157979
100	0.8	16.38055888	3.197953310
110	0.5	10.23784930	3.517748641
120	0.5	10.23784930	3.837543972
130	0.4	8.190279439	4.157339303
140	0.4	8.190279439	4.477134634
150	0.2	4.095139719	4.796929965
160	0.3	6.142709579	5.116725296
170	0	0	5.436520627

Source: Test data St.37 Standards have been processed.

Table 2. Test Steel St.37 Hardening Data

Reading angle (°)	Torque (N.m)	Tension Voltage ($N.mm^{-2}$)	Specific Tapping Angle ($°.mm^{-1}$)
10	0,6	11.82836510	0.324254215
20	12.3	242.4814845	0.648508431
30	20,0	394.2788367	0.972762646
40	22.5	443.5636912	1.297016861
50	24.4	481.0201807	1.621271077
60	25.5	502.7055167	1.945525292
70	26.9	530.3050353	2.269779507
80	28,0	551.9903713	2.594033722
90	28.6	563.8187364	2.918287938
100	29.3	577.6184957	3.242542153
110	30.1	593.3896492	3.566796368
120	30.6	603.2466201	3.891050584
130	31.2	615.0749852	4.215304799
140	31.9	628.8747445	4.539559014
150	32.1	632.8175328	4.863813230
160	32.5	640.7031096	5.188067445
170	33,0	650.5600805	5.512321660
180	33.2	654.5028688	5.836575875
190	33.3	656.4742630	6.160830091
200	33.5	660.4170514	6.485084306
210	33.7	664.3598398	6.809338521
220	34.1	672.2454165	7.133592737
230	34.3	676.1882049	7.457846952
240	34.7	684.0737816	7.782101167
250	34.8	686.0451758	8.106355383
260	35.1	691.9593583	8.430609598
270	35.1	691.9593583	8.754863813
280	35.3	695.9021467	9.079118029
290	35.4	697.8735409	9.403372244
300	20,0	394.2788367	9.727626459
310	1.2	23.65673020	10.05188067

Reading angle (°)	**Torque** (N.m)	Tension Voltage (N.mm^{-2})	Specific Tapping Angle (°.mm^{-1})
320	1.9	37.45648948	10.37613489
330	0.6	11.82836510	10.70038911
340	0.4	7.885576733	11.02464332
350	0.4	7.885576733	11.34889754
360	0.4	7.885576733	11.67315175
370	0.5	9.856970916	11.99740597
380	0.5	9.856970916	12.32166018
390	0.5	9.856970916	12.64591440
400	0.6	11.82836510	12.97016861
410	0.6	11.82836510	13.29442283
420	0.5	9.856970916	13.61867704
430	0.4	7.885576733	13.94293126
440	0.5	9.856970916	14.26718547
450	0.4	7.885576733	14.59143969
460	0.4	7.885576733	14.91569390
470	0.5	9.856970916	15.23994812
480	0.5	9.856970916	15.56420233
490	0.5	9.856970916	15.88845655
500	0.4	7.885576733	16.21271077
510	0.1	1.971394183	16.53696498
520	0.1	1.971394183	16.86121920
530	0.1	1.971394183	17.18547341
540	0	0	17.50972763
540	0	0	17.50972763

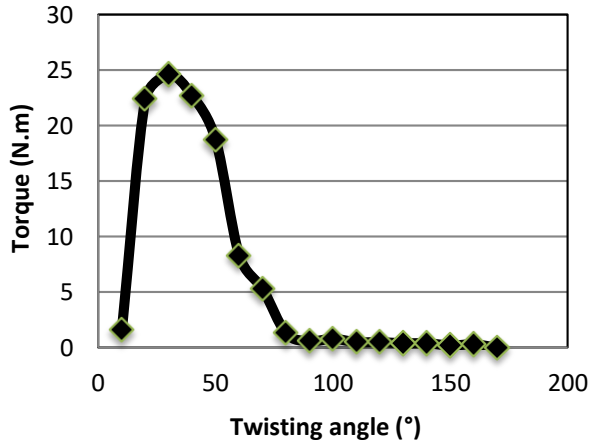

Figure 1. Torque Chart - Twisted Angle St. 37 Standards

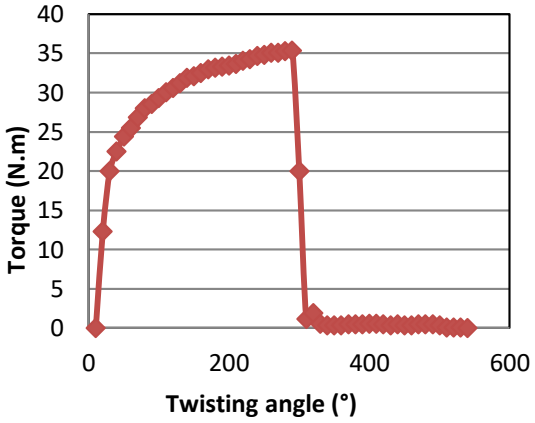

Figure 3. Torque-Twisting Angle St.37 Hardening

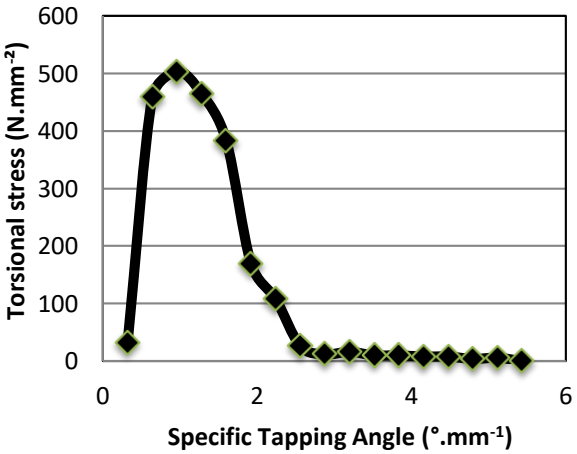

Figure 2. Specific torsional-torsional tension graphs St. 37 Standards

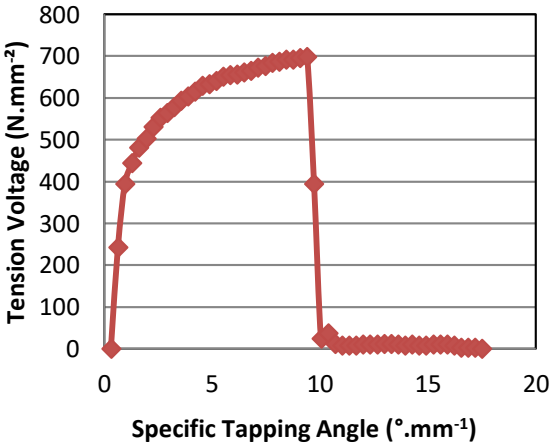

Figure 4. St.37 Hardening specific torsional-torsional tention graph

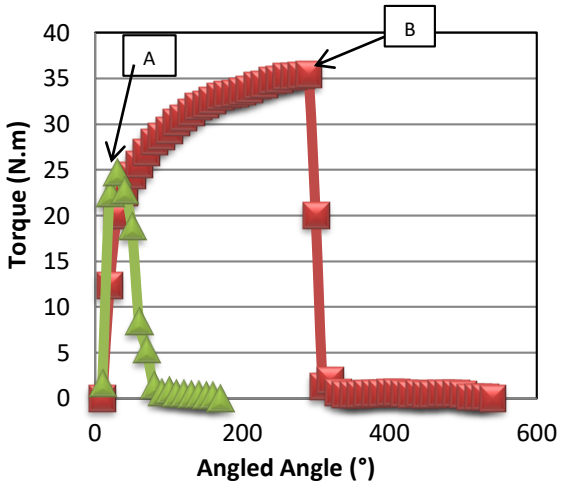

Description: A = St.37 test sample graphs Standard,
B = Graph St.37Hardening test object.

Figure 5. Torque Charts - Twisting angle of both types of specimens

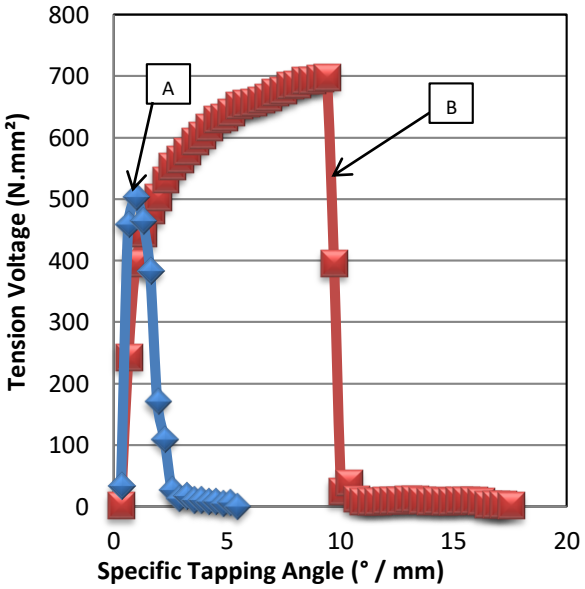

Description: A = St.37 Standard test sample graphs,
B = Graph St.37Hardening test object

Figure 6. Twisted-torsional graphs of specific twisting angles of both types of specimens

3.2 Discussion

As seen the data in the Table 1 and Table 2 and the graphs for the two types of specimens above, it shows the differences in the mechanical properties of each specimen. It turned out that the specimens that were subjected to heat treatment were hardened by a heating process to 800^0C and were cooled quickly using fresh water, their torsional resistance was greater or increased compared to the twisting resistance of the St. 37 standard specimen. The increase in twisting resistance shows in the data above, namely: Maximum steel twist tension St. 37 Standard: 503.7021855 N.mm^{-2} at a maximum torsional moment of 24.6 Nm, whereas, the maximum torsional stress of St.42 Hardening steel: 697.8735409 N.mm^{-2} at a maximum torsional moment of 35.4 Nm. However, the modulus of elasticity (G) of each specimen after calculated using formulas (5) and (6), is obtained: G (St.37 Standard) = 4205.500 (N.mm^{-2}) G (St.37 Hardening) = 1335.750 (N.mm^{-2}).

4. Conclusions

Based on the results of research and data analysis illustrated by graphs, it can be concluded that:

1. Steel St.37 hardening hardened by heating to 800 ºC and chill quickly using fresh water to be more resilient or softer compared to St.37 standard steel. It is evident from the torsional angle St.37 hardening at the proportional boundary equal to 290 degrees, while the torsional angle St.37 The standard at the proportional boundary is 30 degrees. Besides, the torsional moment, twisting tension and the specific torsional angle of the hardened steel have a significant increase. This is shows that there is a significant increase in resistance of twisting.
2. Baja St.37 hardening by heating to 800 ºC and cooled quickly using fresh water, is very useful to obtain shaft material that is more resistant or more resilient to twisting loads when compared to St.37 standard steel

References

[1] A. Zainun, “Elemen Mesin 1”, Bandung, PT. Refika Aditama, 1999.

[2] D.A. Brant, “Metallurgy Fundamentals”, Wisconsien Technical Institute. South Holland Illinois.Industrrial Technology Division Western, 1985.

[3] Daryanto, “Fisika Teknik”, Jakarta, PT. Rineka Cipta, 1997

[4] J.E. Neely, “Practical Metallurgy and Material of Industry”, Second Edition, 1984.

[5] I.K. Rmpung, “Pengaruh Perlakuan Panas Terhadap Ketahanan Puntir Baja (St.42) dengan Temperatur Pemanasan 800 ºC”, Jurnal Logic, 12, 1, 2012.

[6] R.S. Khurmi, dan J.K. Gupta, “A Text Book of Machine Design”, New Delhi, Eurasia Publishing House Ltd, 1982.

Journal of Applied Mechanical Engineering and Green Technology

Journal homepage: http://ojs.pnb.ac.id/index.php/JAMETECH
p-ISSN: 2655-9145; e-ISSN: 0000-0000

Simulation and experimental verification on re-heat two-stage adsorption refrigeration cycle

I.G.A.B. Wirajati[a1], I.B.G. Widiantara[a], and I.N. Ardita[a]

[a]*Mechanical Engineering Department, Politeknik Negeri Bali, Campus Street Bukit Jimbaran, Kuta Selatan, Bali 80364, Indonesia*

Abstract

In this paper, an experimental investigation of re-heat two-stage adsorption cycle is verified by MATLAB simulation, and the working principle of the cycle introduced as well. The objective is to verify the effect of heat source temperature on the performance if chilled water outlet temperature is fixed at 9 ºC in simulation and compared with the experiment. Coefficient of performance and cooling capacity are the performance indicator of the cycle.

Keywords: Re-heat adsorption cycle; COP; cooling capacity; desorber; and adsorber

1. Introduction

Adsorption refrigeration system is one of the environmentally friendly cooling systems because of not only as an alternative for reducing CFCs and HCFCs uses but also as an energy efficient technology and contributes for the green technology [1]. When compared to other cycles, the adsorption cycle has advantages in terms of its ability to use a relatively low heat source which is close to the environment temperature so that temperatures below 100 ºC can be used, which are investigated by Kashiwagi et al [2]. One of the adsorption cycles namely reheat two-stage has been studied by Alam et al [3] and Khan et al [4].

However, chilled water outlet temperature is arranged in fluctuated. Thong et al [5] alleged that it is also important to maintain a constant chilled water outlet temperature in order to increase the conversion efficiency of the system and Wirajati et al [6] conducted the experiment by implementing the fixed chilled water outlet conditions. In this paper, a MATLAB program is developed and compared with the experiment to shown the performance of the cycle. The results show that the performance increased along with heat source temperature and cycle times 2000 – 2500s produces highest cooling capacity.

2. Working Principle of the Cycle

Figure 1 (a) show the reheat two-stage adsorption cycle scheme while Figure 1 (b) shows the P-T-X diagram for standard conditions. The adsorbent heat exchangers of the chiller are operated in a cycle through six thermodynamic processes, namely: adsorption (1-2), mass recovery with cooling (2-3), pre-heating (3-4), desorption (4-5), mass recovery with heating (5-6), and pre-cooling (6-1). In the adsorption-evaporation process, refrigerant (water) in evaporator is evaporated at the temperature (T_{eva}) and seized heat (Q_{eva}) from the chilled water. At the end of each half-cycle, one heat exchanger (HEX-1) is cold and the other one (HEX-2) is hot. Simultaneously, HEX-1 is at low pressure and must be pressurized up to condenser pressure; HEX-2 is at high pressure and must be depressurized down to evaporator pressure. Making up and down of this pressure, vapor is transferred from desorber to adsorber.

This process is known as mass recovery process. Adsorption/desorption process will occur automatically due to a difference in heat exchanger's pressure. HEX-2 pressure increases while HEX-1 pressure decreases. Both HEX pressures reach the same point. To provide more cooling capacity, desorber temperature (HEX-2) is still at high temperature or continuing heating process. Refrigerant release is still occurring from HEX-2 to HEX-1. It causes HEX-2 concentration to decrease. Afterwards, HEX-1 is heated up by hot water and HEX-2 is cooled down by cooling water. During this process, refrigerant circulation is stopped by closing all refrigerant valves. This process is known as pre-heating/pre-cooling process. When the pressures of HEX-1 and HEX-2 are nearly equal to the pressures of condenser and evaporator, the valve between HEX-1 and condenser (as well as the valve between HEX-2 and evaporator) is opened, allowing refrigerant to flow.

[1]Corresponding author. Tel.: +6281338185601; Fax: +62361702811
E-mail address: igabwirajati@pnb.ac.id

Nomenclature

A	Area (m^2)	q*	Concentration equilibrium (kg_{ref} kg_{ad}^{-1})
C	Specific heat (kJ kg^{-1} $^oC^{-1}$)	Q_{st}	Iso-steric heat of adsorption (J kg^{-1})
D_0	Pre-exponential constant (m^2s^{-1})	R	Gas constant (J $mol^{-1}K^{-1}$)
E_a	Activation energy (J mol^{-1})	R_n	Average radius of a particle (m)
L	Latent heat of vaporization (J kg^{-1})	T	Temperature (K)
$\dot{m}$	Mass flow rate (kg s^{-1})	t	Time (s)
P_s	Saturated vapor pressure (Pa)	U	Overall heat transfer coefficient (W m^{-2} K^{-1})
q	Concentration (kg_{ref} kg_{ad}^{-1})	W	Weight (kg)

Adsorption and desorption process then starts. In this process, refrigerant from HEX-1 will be liquefied in condenser by releasing heat condenser to heat sink. Refrigerant liquid flows from condenser to evaporator. In evaporator, refrigerant will be adsorbed iso-barically by HEX-2. Evaporation process occurs and produces cooling effect. Evaporation heat is supplied by flowing chilled water at low heat source temperature. To complete one cycle, the next process is the same as the previous half-cycle. Only, the position of HEX-1 is as desorber and HEX-2 is as adsorber.

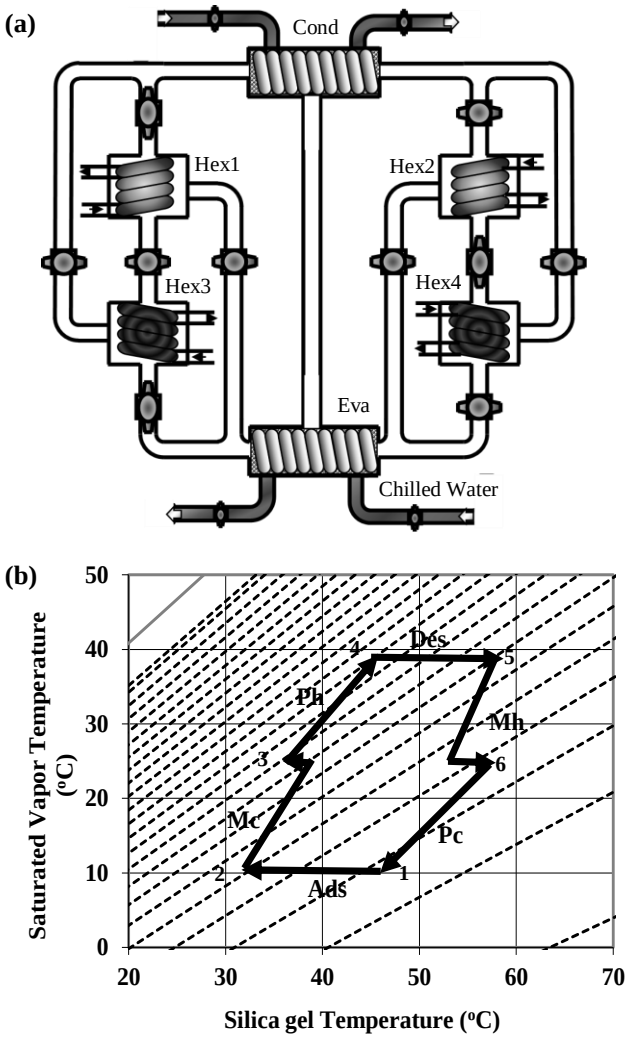

Figure 1. (a) Reheat two stage adsorption scheme and (b) P-T-X Diagram

Table 1. Operational strategy

Hex	Mode									
	A	B	C	D	E	F	G	H	I	J
1		Des		Mh	Pc		Ads		Mc	Ph
2	Mh	Pc		Ads		Mc	Ph		Des	
3		Ads		Mc	Ph		Des		Mh	Pc
4	Mc	Ph		Des		Mh	Pc		Ads	

Ads = adsorption, Des = desorption, Mh = mass recovery heating, Mc = mass recovery cooling, Ph = pre-heating, Pc = pre-cooling

3. Developing Equation

3.1. Heat Transfer in Evaporator, Condenser and Heat Exchanger

Heat transfer in evaporator, condenser and heat exchanger describes as follow:

$$T_o = T + (T_i - T) exp\left(\frac{U_{bed}.A_{bed}}{\dot{m}_w.C_w}\right) \quad (1)$$

$$T_{chill,o} = T_{eva} + \left(T_{chill,i} - T_{eva}\right) exp\left(-\frac{U_{eva}.A_{eva}}{\dot{m}_{ch}.C_{ch}}\right) \quad (2)$$

$$T_{con,o} = T_{con} + \left(T_{cw,i} - T_{con}\right) exp\left(-\frac{U_{con}.A_{con}}{\dot{m}_{cw}.C_w}\right) \quad (3)$$

In this case, T indicates the temperature. The temperature and concentration of the liquid in both Hex, evaporator and condenser are assumed uniform. Specific heat from refrigerant (water) in the liquid phase because the system works in the low concentration range. The temperature of fluid (water), T_i and T_o fluid heat transfer shows cold water and hot water when the process of adsorption and desorption. U and A in the formula state the heat transfer parameters, namely the overall heat transfer coefficient and heat transfer area

3.2. Energy Balance in Evaporator, Condenser and Heat Exchanger

Energy balance in evaporator, condenser and heat exchanger express below:

$$(W_s.C_s + W_s.C_w.q + W_{bed}.C_{bed})\frac{dT}{dt} = W_s.Q_s\frac{dq}{d_t} - W_s.C_v.\delta[\gamma(T-T_{eva}) + (1-\gamma)(T-T_{wv})]\frac{dq}{dt} + \dot{m}_w.C_w.\varepsilon_{bed}(T_i - T) \quad (4)$$

$$\left(W_{eva,w}.C_w + W_{eva,bed}.C_{eva,bed}\right)\frac{dT_e}{dt} = \dot{m}_{chill}.C_{chill}.\varepsilon_{eva}\left(T_{chill,i} - T_{chill,o}\right)W_s\left(\frac{dq_{ads}}{dt} + \frac{dq_{des}}{dt}\right)(L + C_v(T_{con} - T_{eva}) \quad (5)$$

$$\left(W_{con,w}.C_w+W_{con,bed}.C_{con,bed}\right)\frac{dT_c}{dt}=\dot{m}_{cw}.C_w.\varepsilon_{con}\left(T_{cw,i}-T_{cw,o}\right)-W_s\left(\frac{dq_{des}}{dt}+\frac{dq_{des}}{dt}\right)(L+C_v(T_{des}-T_{con}) \quad (6)$$

Where δ either 0 or 1 depends on whether the adsorbent functions as desorber or adsorber and γ either 1 or 0 depending on whether Hex is connected to the evaporator or with another Hex. The left side of the adsorber/desorber energy balance equation in equation (4) gives the amount of sensible heat needed to cool or heat the silica-gel (s), water (w) and the heat exchanger (hex) metal part during the adsorption or desorption process. This term takes into account the sensible heat input / output required when the cycle operates in accordance with the stages of the process. The first term on the right side of equation (4) is the release of heat from adsorption or heat desorption input, while the second term for sensible heat from steam is adsorbed. The last term on the right side of equation (4) refers to the total amount of heat released into cooling water after the adsorption process or provided by hot water for the desorption process. Equation (4) does not take into account the loss of external heat to the environment because all layers are considered well isolated. The term ε in equations (4.5 and 6) states the effectiveness of the heat exchanger derived from the log difference in the average temperature of the heat exchanger (hex, evaporator and condenser) in the flow system.

The left side of Equations (5 and 6) represents the sensible heat needed by liquid refrigerant and metal tube heat exchanger in the evaporator and condenser. The first term on the right side of equation (5) represents the total amount of heat from cold water and in equation (6) gives the amount of heat released into the cooling water. The second term in equation (5) describes explaining the latent heat of evaporation (L) for the amount of adsorbed refrigerant (dq_{ads}/dt) and the sensible heat needed to cool the incoming condensate from the T_{con} condensation temperature to the T_{eva} evaporation temperature, while the second term equation (6) describes the latent heat of evaporation (L) for the amount of refrigerant absorbed (dq_{des}/dt) and the amount of heat carried by the liquid condensate when it leaves the condenser to the evaporator

3.3. Performance Indicator

The performance of a re-heat two-stage adsorption chiller is mainly characterized by cooling capacity (CC), coefficient of performance (COP), and can be measured by the following equations:

$$Cooling\ Capacity = \dot{m}_{chill}C_w\int_0^{t_{cycle}}\left(T_{chill,in}-T_{chill,out}\right)dt/t_{cycle} \quad (5)$$

$$COP=\frac{\dot{m}_{chill}C_w\int_0^{t_{cycle}}(T_{chill,in}-T_{chill,out})dt}{\dot{m}_{hot}C_w\int_0^{t_{cycle}}(T_{hot,in}-T_{hot,out})dt} \quad (6)$$

3.4. Total Energy Balance

The total mass balance of refrigerant (water) can be expressed as:

$$W_{eva,w}=-W_s\left(\frac{dq_{des\text{-}con}}{dt}+\frac{dq_{ads\text{-}eva}}{dt}\right) \quad (7)$$

3.5. Adsorption Rate

The combination of silica-gel adsorption rate was modeled as a function of temperature [7]:

$$\frac{d_q}{d_t}=k_sa_p\ .\left(q^*-q\right) \quad (8)$$

The overall mass transfer coefficient, k_sa_p, was estimated by Eq.(9) and (10), as below:

$$k_sa_p=\frac{15D}{R_p^2} \quad (9)$$

$$D=D_0\ \exp(-E_a/RT)\frac{dq}{d_t}=k_sa_p\ .(q^*-q) \quad (10)$$

The amount adsorbed in equilibrium, q*, is predicted by equation as follows:

$$q^*=\frac{0.8\ x\ [P_s(T_w)/P_s(T_s)]}{1+0.5\ x\ [P_s(T_w)/P_s(T_s)]} \quad (11)$$

where $P_s(T_w)$ and $P_s(T_s)$ are the saturation vapor pressure at temperature Tw (water vapor) and Ts (silica gel), respectively. The saturation vapor pressure and temperature are correlated by Antoine's equation, as follows:

$$P_s=133.32\ x\ \exp\left(18.3-\frac{3820}{T-46.1}\right) \quad (12)$$

4. Results and Discussion

The MATLAB simulation program was developed to identify the performance and compared with the experiment. Both simulation and experiment were operated based on the Table 1 and Table 2.

4.1. Temperature Histories of Heat Exchanger (Bed)

Figure 2 has shown the temperature histories of Bed in both simulation and experiment. Heat source temperature 75°C and total cycle time 1300s are chosen

Table 2. Standard operating conditions of the simulation and experiment

	Temperature (°C)	Flow rate (simulation) (kg.s^{-1})	Flow rate (experiment) (kg.s^{-1})
Hot water	75	0.364	0.51
Cooling Water	30	0.8	1.4
Chilled water	14	0.364	0.51
Cycle time	1300 s = (420 + 30 + 200) x 2		
	(Ads/Des + Ph/Pc + Mc/Mh) x 2		

Ads/Des : Adsorption-Desorption time
Ph/Pc : Preheating-Precooling time
Mc/Mh : Mass recovery cooling & heating time

In the beginning (420s), mode A into mode C, Bed1 in desorption process, and therefore the temperature of HEX1 increased. In mode D, Bed1in mass recovery with heating process. The temperature of Bed1 decreased suddenly and after that the temperature of Bed1is increased due to heating by hot water. In mode E, Bed1 in pre-cooling process, so that temperature of Bed 1 decreased.

Table 3. Parameter's values in simulation

Symbol	Value	Unit
C_s	924	J/kg K
C_v	1.89E+03	J/kg K
C_w	4.18E+03	J/kg K
D_o	2.54E-4	m^2/s
E_a	2.33E+06	J/kg
L_w	2.50E+06	J/kg
Q_s	2.86E+06	J/kg
R	4.62E+2	J/kg K
R_p	3.00E-04	m
UA_{ads}	2.00E+3	W/m^2K
UA_{des}	2.23E+3	W/m^2K
UA_{eva}	2.36E+3	W/m^2K
UA_{con}	4.06E+3	W/m^2K
W_s	16	kg
$W_{con,w}$	5	kg
$W_{eva,w}$	25	kg

The next process is adsorption process for Bed 1 (mode F, G and H). In this process, Bed 1 operates in evaporator pressure. Refrigerant in evaporator will be evaporated and adsorbed by Bed1. In mode I, Bed1 is in mass recovery with cooling process. The temperature of Bed 1 increased slightly and after that the temperature of Bed 1 is decreased due to cooling by cold water. In mode J, Bed1 in pre-heating process, so that temperature of Bed1 increased.

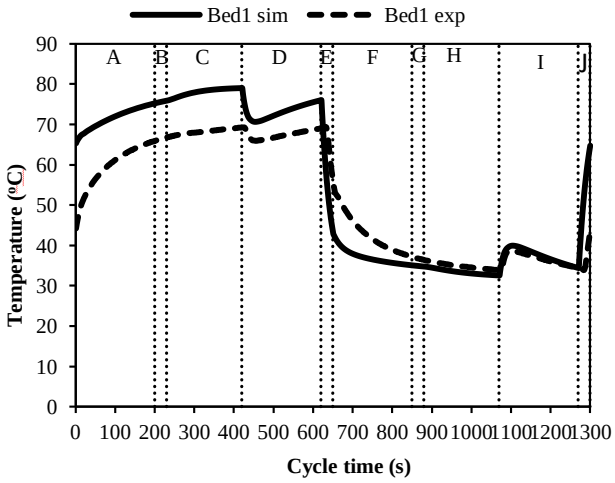

Figure 2. Temperature histories of bed

4.2. Pressure Histories of Heat Exchanger (Bed)

Figure 3 illustrates the pressure histories of the four adsorbent beds (heat exchangers) with heat source temperature is 60oC and total cycle time is 2000s. It is worth to mention here that in the beginning (300s) heat exchangers 2 and 4 are in mass recovery process (340s) where bed 2 is in heating mode and bed 4 in cooling mode (30s). It is seen that in the beginning of mass recovery process, the temperature of bed 2 decreased and that of bed 4 increased though the bed 2 and bed 4 are in heating and cooling mode, respectively. In the beginning of mass recovery process, the saturation pressures of beds change suddenly, so that bed 2 starts to desorb and bed 4 to adsorb water vapor very fast. Therefore, temperature of bed 2 decreased and that of bed 4 increased for few seconds in the beginning of mass recovery process and then the temperature of bed 2 starts to increased and that of bed 4 start to decreased. It is also seen that after half cycle (1000s), temperature of bed 1 and bed 3 did not reach near to inlet hot and cooling water temperature, respectively.

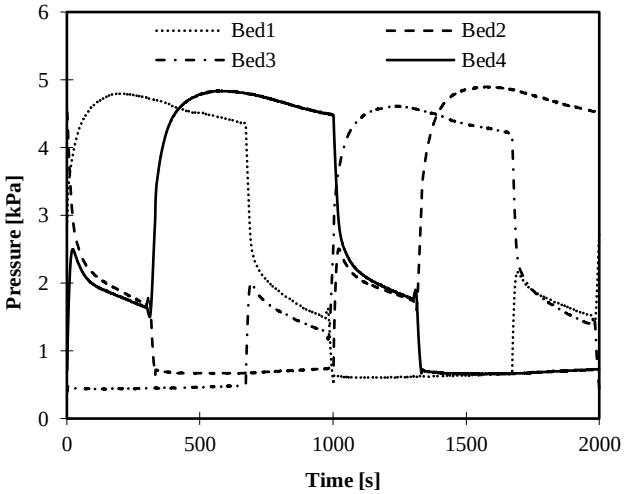

Figure 3. Pressure histories of bed

After mass recovery process, pre-heating and pre-cooling process will occur. Bed 2 is in cooling process and Bed 4 in heating process. Temperature of Bed 2 will decrease during the process of pressure decline and temperature of Bed 4 will increase respectively. The next process is desorption-adsorption process (mode C, D, E). In this process, Bed 2 operates in evaporator pressure. Refrigerant in evaporator 2 will be evaporated and adsorbed by Bed 2. Bed 4 operates in condenser pressure. Refrigerant will be released in desorption process and will be condensed in condenser. Up to mode E is a half-cycle, the next process (F-J) is similar to mode A-E, only adsorber and desorber position will change for each bed pairs.

4.3. Effect of Heat Source Temperature on Performance

The effect of heat source temperature on the coefficient of performance (COP) and cooing capacity are presented in Figure 4 and 5 respectively. Chilled water outlet temperature was 9 ºC and total cycle time was 1300s. COP and cooling capacity both increased along with heat source temperature.

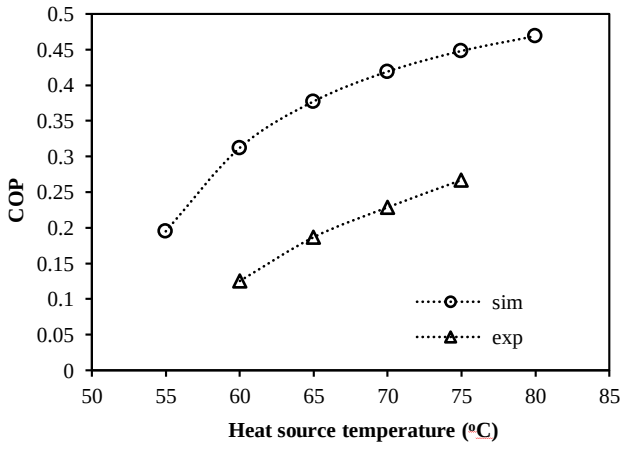

Figure 4. Effect of heat source temperature on COP

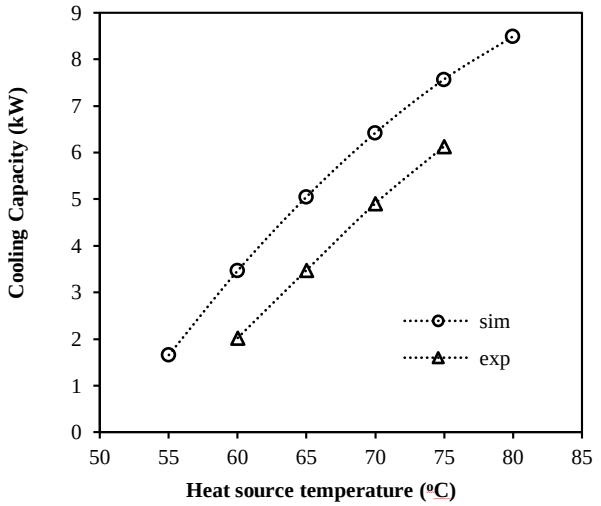

Figure 5. Effect of heat source temperature on performance

The same tendencies are shown in both simulation results compare with the experiment results. Performance simulation is bigger than experiment because there is always some heat loses to the environment in a real system, which is neglected in simulation model.

4.4. Effect of Cycle Time on Performance

The effect of cycle time on performance (COP and cooling capacity) described in Figure 6. Seven cycles times are chosen from 1000s to 4000s. As consideration, the experimental and simulation conditions were set up at the same condition as heat source temperature and chilled water outlet temperature were at 60°C and 9°C, respectively.

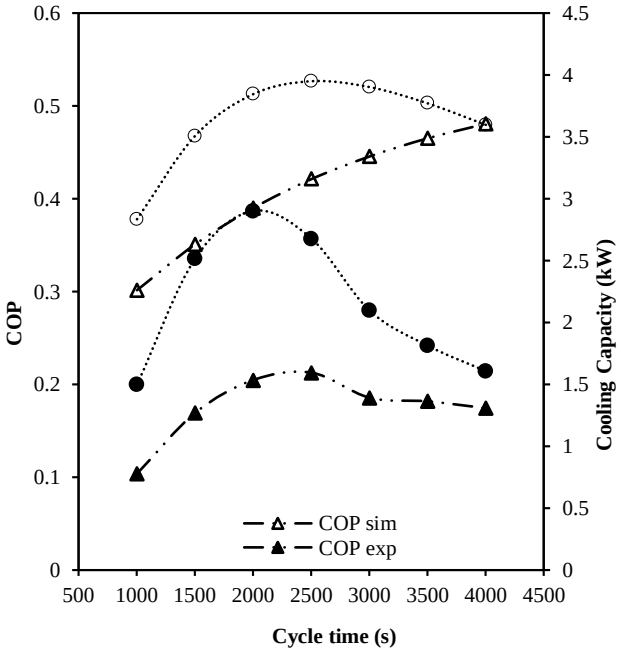

Figure 6. Effect of cycle time on performance

4.5. The average of chilled water out temperature and mass flow rate

As can be shown in simulation results that the trend of the average chilled water out is flat smoothly because it is easy to give the mass flow rate values in simulation to reach the chilled water out 9°C. The tendency became different in the experiment results because it is a little bit difficulties to control mass flow rate to gain chilled water out 9°C. From Figure 2 (b) we can say that in order to gain chilled water out 9°C, we must increase mass flow rate if heat source temperature increased.

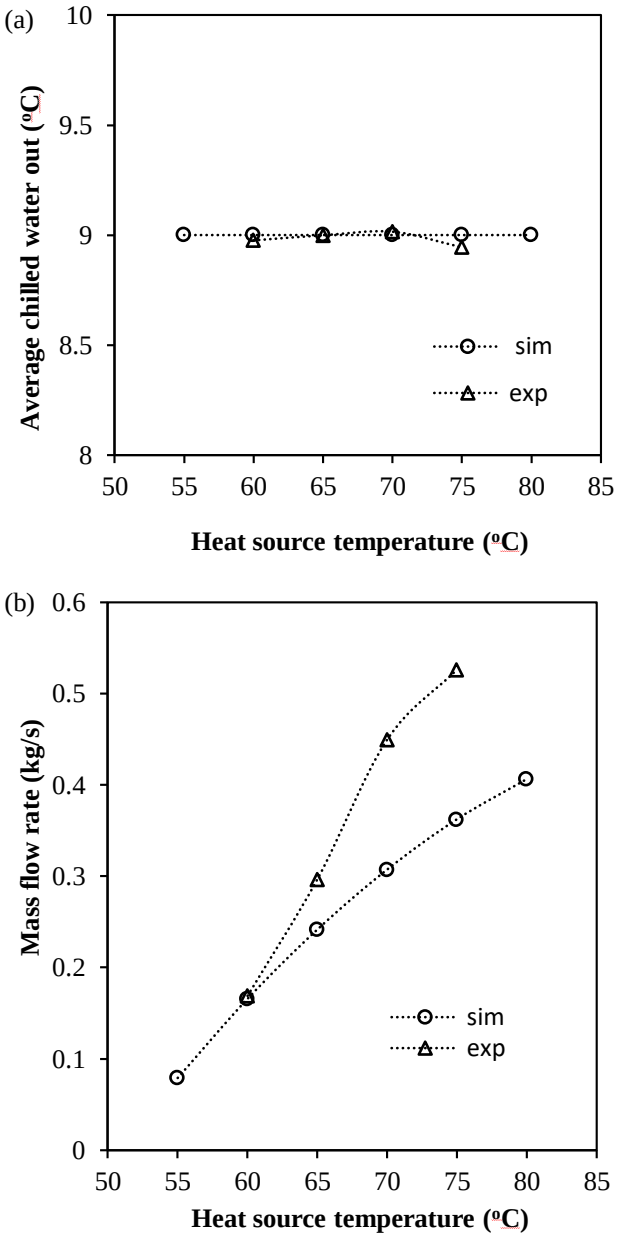

Figure 7. (a) Average chilled water out (b) Mass flow rate behavior of the chiller

5. Conclusions

The following concluding remarks can be drawn from the present study.

(a) In both experiment and simulation are showing the same tendency results.
(b) COP and cooling capacity increased along with heat source temperature.
(c) Cycle times within 2000 – 2500s produces highest cooling capacity.

References

[1] A.O. Dieng , R.Z. Wang, "Literature review on solar adsorption technologies for ice-making and air conditioning purposes and recent developments in solar technology", Renewable and Sustainable Energy Reviews, 5, 2001, pp. 313-342.

[2] T. Kashiwagi, A. Akisawa, S. Yoshida, K.C.A. Alam, and Y. Hamamoto, "Heat driven sorption refrigerating and air conditioning cycle in Japan", Proceedings of the International Sorption Heat Pump Conference, Shanghai, China, 2002, pp. 50–62.

[3] K.C.A. Alam, M.Z.I. Khan, A.S. Uyun, Y. Hamamoto, A. Akisawa, T. Kashiwagi, "Experimental Study Of A Low Temperature Heat Driven Re-Heat Two-Stage Adsorption Chiller", Appl. Therm. Eng., 27, 2007, pp. 1686–1692.

[4] M.Z.I. Khan, K.C.A. Alam, B.B. Saha, A. Akisawa, T. Kashiwagi, "Study On A Re-Heat Two-Stage Adsorption Chiller - The Influence Of Thermal Capacitance Ratio, Overall Thermal Conductance Ratio And Adsorbent Mass On System Performance", Appl. Therm. Eng., 27, 2007, pp. 1677–1685

[5] C.H. Tong, N.K. Choon, A. Malek, T. Kashiwagi, A. Akisawa, B.B Saha, "A Regenerative Adsorption Process And Multi Reactor Generative Adsorption Chiller", Espacenet Description:EP 1140314 (A1).

[6] I.G.A.B. Wirajati, A. Akisawa, Y. Ueda, and T. Miyazaki, "Experimental Investigation of a Reheating Two-Stage Adsorption Chiller Applying Fixed Chilled Water Outlet Conditions", Heat Transfer Research, 46, 2015, pp.293-309.

[7] A. Sakoda, and M. Suzuki "Fundamental Study on Solar Powered Adsorption Cooling System", Journal Chemical Engineering of Japan, 17, 1984, pp. 52–57.

Journal of Applied Mechanical Engineering and Green Technology, Vol. 1, No. 1 (2019) 31-34

Journal of Applied Mechanical Engineering and Green Technology

Journal homepage: http://ojs.pnb.ac.id/index.php/JAMETECH
p-ISSN: 2655-9145; e-ISSN: 0000-0000

Design of brake bleeding tool for four wheeled vehicles using pneumatic system

I.N. Ludra Antara[1]

Mechanical Engineering Department, Politeknik Negeri Bali, Campus Street Bukit Jimbaran, Kuta Selatan, Bali 80364, Indonesia

Abstract

Used bottles and pipes are the tools that have been utilized in the manual process of bleeding. There are several weaknesses in using these tools for bleeding, thus there is a need to create a new design using the existing tools. With the used bottles and pipes, a great amount of energy is needed to pump the brake pedal, and two people are needed for the job. Furthermore, the use of used pipes and bottles is less efficient because it requires a longer time to complete the bleeding process. Upon evaluating this issue, a tool to complete the bleeding process more effectively and efficiently is needed. Thus, the tool to minimize the need of more mechanics in the bleeding process is important. For this, the brake bleeding tool for 4 wheeled vehicles using the pneumatic system is designed. This tool utilize the vacuum resulted from the T junction, and with it, an effective and efficient bleeding process is attained. It is especially efficient in terms of manpower because one person is enough to finish the job, and the bleeding process time is more efficient. Based on the test conducted, the average time needed to manually bleed a vehicle is 542 seconds. As for the brake bleeding tool for 4 wheeled vehicles using the pneumatic system, the average time needed is 389 seconds. The test results show that the design created is able to accelerate the bleeding process by 28,2% faster than the manual method.

Keywords: Bleeding; brake; T-junction; reservoir tank; and vehicle

1. Introduction

With the current rapid development of technology, which includes the technology in the automotive world, there has been no end to new inventions. Innovation after innovation, continuous development has been seen in order to make the vehicles better. Better in terms of performance, fuel efficiency, comfort and safety. As vehicles are one of the equipment which support daily activities and there has been an increasing number of four wheeled vehicles used, automotive producers continuously try to improve the vehicle's systems to enhance the comfort and safety for the passengers. One which needs to be given attention is the brake maintenance system.

The importance of maintaining and fixing the brake system is to prevent any damage on the components. In the process of fixing and assembling the components, there certainly are air trapped in the brake system. As a result, the brakes cannot function well because the liquid fluids are incompressible. This means that even if the liquid fluid receives pressure, its volume will not change. On the other hand, gas fluid are compressible, which means that with pressure, its volume will change or will be compressed.

The air that are trapped in the brake system will cause the braking process to be not optimal. This is because when the brake pedal is pressed, the braking process will not directly occur as the air is compressible in the brake system. Thus, this may endanger the driver. The method to release the air is called bleeding. Manual bleeding is performed by two mechanics, in which one mechanic opens or closes the nipple bleeder and the other mechanic pumps the brake pedal. Manual bleeding is performed by pumping the brake pedal several times until it feels hard or dense, then hold the brakes and open the nipple bleeder so that the brake oil can be released from the nipple bleeder. This is conducted several times until the air has been dispensed through the bleeding pipe. This method is less effective because it must be performed by two mechanics and requires a great amount of energy and time.

In line with the background of the issue, innovation is the main key in designing a tool that is capable of enhancing the efficiency of the mechanic's job, especially in the process of releasing the air from the brake system. This tool is designed to minimize the required manpower, in other words one person can complete the job, and to improve the time and energy efficiency in completing the process.

[1]Corresponding author. Tel.: +62361701981; Fax: +62361702811
E-mail address: nengahludraantara@pnb.ac.id

The purpose of this design is to examine the brake bleeding process, specifically for 4 wheeled vehicles using the pneumatic system, and to determine whether it really is effective and efficient in bleeding compared to the manual method.

An engineering design is a form of construction or structure which transforms concepts into items or tools. According to [1] there are some criteria which must be considered in planning and designing a construction, among others determining the need, selecting the form and mechanism, selecting the material, and determining the size. Brakes are designed to decelerate speed and stop the vehicle or allowing the vehicle to park in a declining surface. It is also a safety tool which ensures that the vehicle is safe. Machines transform heat energy into kinetic energy to move the vehicle. Whereas the working principle of brakes is to revert kinetic energy into heat energy to stop the vehicle. In general, brakes work because of the pressure coupling system against the rotation system, and the braking effect is attained from the friction between two objects [2]. The break system can be distinguished into two, first the hydraulic brake system which is a brake distribution system using liquid. The liquid used is a type of fluid that has a high durability.

The hydraulic brake system works based on Pascal's law which states that "pressure exerted on liquid in an enclosed room will be distributed evenly towards all directions". This shows that when the brake pedal is pressed, the pressure will be distributed to the brake actuator with a magnitude in line with the force exerted by the driver on the brake pedal [3]. Second is the drum brake system which works by distributing the force exerted by the driver on the brake pedal mechanically to the master cylinder. This will cause the liquid in the master cylinder to be pressured and distributed to the wheel cylinders for the drum brake. From the wheel cylinder, it will be forwarded to the canvas brake so the canvas brake pressures the drum and decelerates the vehicle's movements, whereas the disc from the master cylinder will be forwarded to the caliper.

2. Method

The brake bleeding tool for 4 wheeled vehicles using the pneumatic system is designed to ease the work of mechanics, be more time efficient, and manpower efficient. With the design of this tool, mechanics do not need to pump the brake pedal, thus bleeding can be done by one mechanic, such as shown in Figure 1. The working principle of the brake bleeding tool for 4 wheeled vehicles using the pneumatic system is by utilizing the vacuum in the T junction which is distributed to the reservoir tank and connected to the flexible pipe which is inserted to the vehicle's brake nipple.

The design and construction include some steps in the process of designing the brake bleeding tool for 4 wheeled vehicles using the pneumatic system [4,5,6], in which are: (i) Conducting observations or surveys on several mechanic workshops, in order to assess directly the brake system's bleeding process for 4 wheeled vehicles; (ii) References, in which are books related to the brake system and design.

The data collection method utilized in this research was the observation method or direct experiment on the vehicle, in which the data is collected using a time measuring tool, a stopwatch. The study is planned to use the Daihatsu Xenia 2016 vehicle as this vehicle is commonly used by many people.

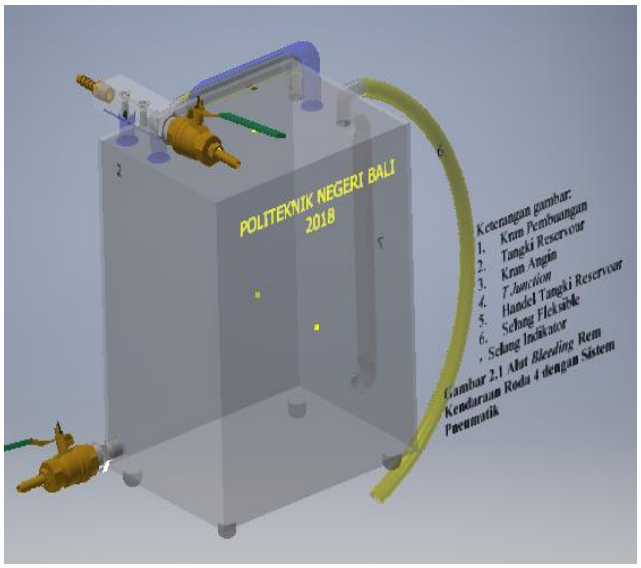

Figure 1. The design of the brake bleeding tool

The execution stage of creating the brake bleeding tool for 4 wheeled vehicles using the pneumatic system is described in the form of schemes which briefly explain the steps conducted in creating the tool, starting from the planning step until the tool is completely produced such as shown in Figure 2.

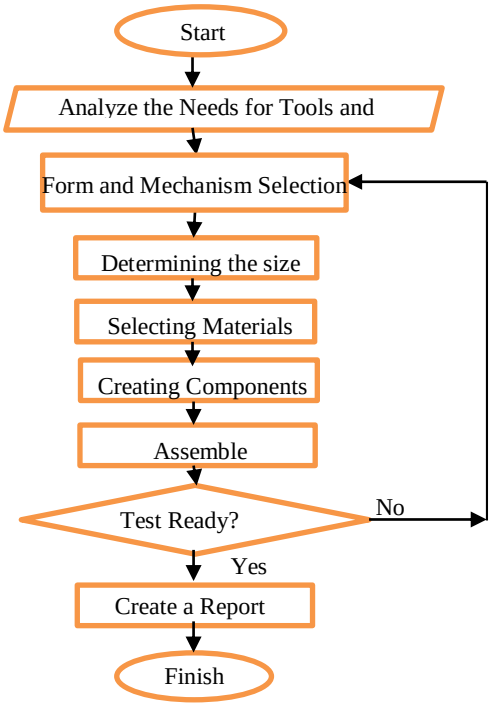

Figure 2. The execution stage of creating the brake bleeding tool

4. Results

Based on the survey results, the brake bleeding tool for 4 wheeled vehicles using the pneumatic system is needed to conduct the vehicle bleeding process efficiently and practically. The working system (as shown in Figure 4)

starts with the air pressure from the compressor entering through the coupler connector and through the T junction, which works similarly to a venturi on carburetors. When the pressurized air enters the venturi pipe, the air speed will increase resulting in the decrease in air pressure. Consequently, there is a vacuum due to the difference in pressure between the divider pipe and the venturi, as both gas and liquid fluid flows toward lower pressures. The vacuum is then distributed to the reservoir tank, and directed to the L junction through the flexible pipe which is used to absorb the brake oil liquid, thus releasing it to the reservoir tank.

The components needed to form the mechanisms, in line with the function and working principle of the brake bleeding tool for 4 wheeled vehicles using the pneumatic system, are: L Junction, Flexible Pipe, Straight Connector, ¼ Wind Faucet, Plate, Coupler Connector, T Junction, Rubber Feet, Bolts and Nuts, Reservoir Tank, Tank Indicator, a stand for the T Junction, Straight Connector and L Junction.

The proses of creating the components of the brake bleeding tool for 4 wheeled vehicles using the pneumatic system utilizes machineries such as: bending machine, electric weld machine, stand drilling machine, grinder, and others [7]. Aside from the machineries, hand tools are also needed in the process of making the components. The components are made referring to the shop drawing. The production process of each component is as follows:

- Prepare the tools and materials that will be used;
- First cut the plate into two parts with a dimension of 55 cm x 23 cm and 63 cm x 15 cm.
- Drill the plate with a 6,5 mm drill, used for the reservoir indicator. A 10 mm drill is used to fasten the L Junction and the straight connector.
- Afterwards, bend the plate with a bending machine.
- Weld the nut on the upper hole to fasten the L Junction and Straight Connector.
- Weld the plate that has been bent earlier, and in welding try to make it without any holes or leaks.
- Afterwards, prepare the L shaped pipe and weld it for the reservoir tank indicator, which will be connected to the pipe.
- Make a stand for the T Junction with a height of 3 cm, length of 6 cm, and a width of 3 cm. Drill the stand in accordance with the T Junction.
- Create a reservoir tank handle to hold and move the tank using a round iron with a height of 4 cm and length of 12 cm.
- Weld the 4 bolts on the bottom part of the tank to hold the feet rubber. Using bolt 8 with a 1 cm length is enough.
- Grind the tank parts after the weld process in order to make it smooth. Afterwards conduct the leakage test on the tank. If there are any leakages, weld and grind the tank again.
- After the tank is free from any leakage, continue with the sealing or covering process.
- Use sandpaper on the tank parts until the surfaces are even and smooth.
- Continue with the painting process.

The Assembling Process can be described as below:

- Prepare all components for the brake bleeding tool for 4 wheeled vehicles using the pneumatic system.
- Assemble the T Junction. To do this, first attach the wind faucet on the entrance pipe of the T Junction, then assemble the coupler connector to connect it to the compressor pipe. Afterwards, fasten the wind outlet and assemble the straight connector to connect the T Junction with the reservoir tank (Figure 3).

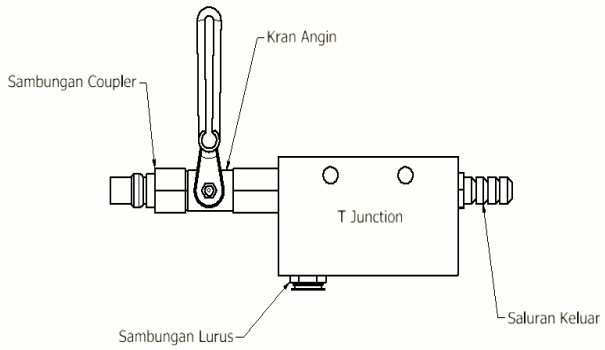

Figure 3. Assembling the T Junction

- Fasten the clear hose for the reservoir tank indicator and tighten it with clamps.
- Fasten the drain faucet on the reservoir tank. Before fastening it, attach seal tape on the drat faucet to prevent leakages.
- Attach the L Junction and the straight connector on the reservoir tank, add in enough seal tape.
- Fasten the T Junction on its stand and tighten it up using bolts. Afterwards, connect the straight connector on the T Junction to the straight connector on the reservoir tank with a pipe.
- Fasten a pipe on the L junction which will be connected to the brake nipple to absorb the brake fluid.
- After that fasten the feet rubber on the reservoir tank and tighten it with bolts.
- The brake bleeding tool for 4 wheeled vehicles using the pneumatic system is ready to be used (such as shown in Figure 4).

Figure 4. Production Results of the brake bleeding tool for 4 wheeled vehicles using the pneumatic system

The test for the brake bleeding tool for 4 wheeled vehicles using the pneumatic system is conducted on 3 mechanisms by comparing the speed in completing the bleeding process, using tools and manual method. The test results for the bleeding process using the tool and manual method are identical as shown in the Table 1.

Table 1. Test for the Tool

No.	Experiment	Time required to complete the bleeding process	
		With bleeding tool	Manual method
1	Experiment 1	119 seconds	175 seconds
		126 seconds	169 seconds
		132 seconds	183 seconds
2	Experiment 2	121 seconds	155 seconds
		116 seconds	160 seconds
		121 seconds	161 seconds
3	Experiment 3	130 seconds	180 seconds
		126 seconds	180 seconds
		133 seconds	182 seconds
4	Experiment 4	140 seconds	200 seconds
		137 seconds	203 seconds
		155 seconds	220 seconds
Average		389 seconds	542 Seconds

By comparing the bleeding time using the manual method and the brake bleeding tool for 4 wheeled vehicles using the pneumatic system, the percentage of time saved in the bleeding process is as follows:

$$\% = \frac{\text{Manual bleeding time} - \text{bleeding time using the tool}}{\text{manual bleeding time}} \text{ x } 100\%$$

$$\text{Percentage} = \frac{542 \text{ seconds} - 389 \text{ seconds}}{542 \text{ seconds}} \text{ x } 100\%$$

$$= 28{,}2\ \%$$

Thus, the percentage of time saved in the bleeding process with a brake bleeding tool for 4 wheeled vehicles using the pneumatic system is 28,2%. The bleeding process with the brake bleeding tool for 4 wheeled vehicles using the pneumatic system is shown to be more efficient and practical.

5. Conclusions

The shape of the brake bleeding tool created for 4 wheeled vehicles using the pneumatic system which can be seen in Picture 3.3. by utilizing the T Junction creates a vacuum or absorption. The working principle is similar to the venturi in carburetors. When the pressured air flows through the venturi, the speed of the air will increase resulting in the fall in air pressure. The difference in pressure in the divider pipe with the venturi results in vacuum or absorption because the gas and liquid fluids will flow towards lower pressure regions.

Based on the test results, the average time needed to bleed a vehicle manually is 542 seconds, while the average time needed with the brake bleeding tool for 4 wheeled vehicles using the pneumatic system is 389 seconds. The test results show that the design created can accelerate the bleeding process by 28.2% compared to the manual method. This design is also more effective and practical in terms of manpower because it can be done by one mechanic.

References

[1] Z. Achmad, "Elemen Mesin I", Bandung:PT.Refika Aditama, 2006.

[2] Tim Toyota, "New Step 1 Training Manual", Conference, PT. Toyota Astra Motor, 2003.

[3] Sularso dan H. Tahara, "Pompa dan Kompresor", PT. Pradnya Paramita, Jakarta, 2000.

[4] R. Ginting, "Perancangan Produk", Graha Ilmu. Yogyakarta, 2010.

[5] Y.F. Huda, "Mahir Menggunakan Autodesk Inventor Pro 2013", Adi Yogyakarta, 2013.

[6] G.T. Sato, and H.N. Sugiarto, "Menggambar Mesin", PT. Pradnya Paramita, 1986.

[7] M. Suratman, "Teknik Mengelas Asitilin, Brazing, dan Las Busur Listrik", Edisi 1. Pustaka Setia, 2001.

Journal of Applied Mechanical Engineering and Green Technology

Journal homepage: http://ojs.pnb.ac.id/index.php/JAMETECH
p-ISSN: 2655-9145; e-ISSN: 0000-0000

Effects of water content in a-zeotropic ethanol to the power, specific fuel consumption and thermal efficiency of an SI engine

I.M. Suarta[a1], I. P. G. Sopan Rahtika[a], P.W. Sunu[a], K. Bangse[a], and I.N. Darma Susila[a]

[a]*Mechanical Engineering Department, Politeknik Negeri Bali, Campus Street Bukit Jimbaran, Kuta Selatan, Bali 80364, Indonesia*

Abstract

In this research, the effect of water content in a-zeotropic ethanol to the power produced, specific fuel consumption, and the thermal efficiency of an SI engine was observed. Tests carried out on anhydrous ethanol fuel (99.7% v) and a-zeotropic ethanol fuel (95.5% v). The test was carried out using the engine brake power indicator load cell type TD 800PM. The amount of power produced, specific fuel consumption and engine thermal efficiency were tested for varying load on four stroke one-cylinder engine. The amount of power, specific fuel consumption was observed, also the thermal efficiency produced by both of the fuels was calculated. The amount of power, specific fuel consumption and thermal efficiency using both types of fuel compared. The results showed that the amount of power produced by a-zeotropic ethanol fuel was higher than anhydrous ethanol fuel. The need for specific fuels when uses a-zeotropic ethanol slightly higher than anhydrous ethanol. Engine thermal efficiency produced by a-zeotropic ethanol is lower than anhydrous ethanol.

Keywords: ethanol; anhydrous; a-zeotropic; fuel; efficiency

1. Introduction

Energy saving, global warming and air pollution are the main reasons for the use of renewable alternative energy and environment friendly [1, 2, 3, 4, 5]. Ethanol can be used directly as a fuel, or mixed with gasoline in a SI engine [4, 6]. The use of anhydrous ethanol as fuel requires very high energy in its purification process. One of several ways to make ethanol more competitive as fuel is to use it with a higher water content [7, 8]. A-zeotropic ethanol is ethanol with a concentration of 95.5% v. A-zeotropic ethanol can be produced by distillation without molecular sieves. The combustion speed and flammability limit (ER) of a-zeotropic ethanol are also better than anhydrous ethanol [9, 10]. Testing of short chain alcohol fuels such as methanol, ethanol and butanol has been carried out a lot to reduce fossil fuel uses, improve the emissions quality and reduce toxic exhaust gases. Differences in property of alcohol fuels cause variations in consumption, performance and emissions of gasoline and diesel engines [2, 11].

The research uses a fuel mixture of gasoline with ethanol is also done by [12]. In their study tested engine performance and exhaust emissions produced. His research claims that addition of ethanol increases engine power, this can be related to the presence of hydroxyl radicals in ethanol, which contribute to complement combustion enhancer. Extra oxygen in the molecular structure of ethanol caused more release of chemical energy as result of combustion of fuel converted to thermal energy. BSFC of the engine is increases by 22.81% with the addition of 10% ethanol to gasoline as shown in Figure 1.

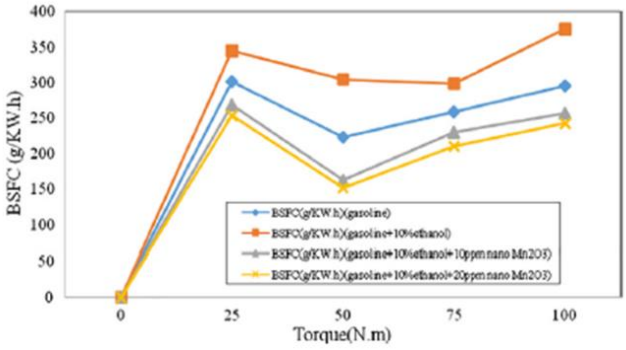

Figure 1. Effect of gasoline blends with ethanol and Mn_2O_3 on BSFC

Engine performance test using ethanol fuel is also done by [13]. The test concluded that ethanol with 5%v of water content was operated at engine with constant speed 3,600 rpm, stoichiometric mixture showed a load effect on BSFC and efficiency. By increasing the generator load from 10% to 100%, overall efficiency increased by 18%, while BSFC

[1]Corresponding author. Tel.: +6281236455857; Fax: +62361702811
E-mail address: madesuarta@pnb.ac.id

Nomenclature

SI	Spark ignition	TDV	Total displacement volume (m^3)
BSFC	Brake specific fuel consumption		

decreased by around 76%. A decreasing trend of BSFC when increasing load also indicated by [14]. The emissions are very low. The results of the study can be seen in Figure 2.

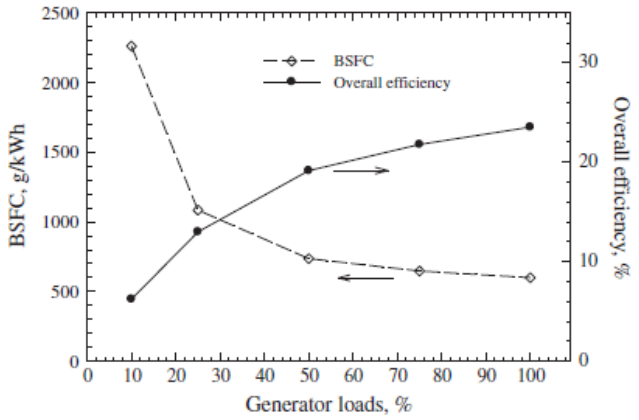

Figure 2. Effect of load on BSFC and efficiency when using ethanol fuel 95% v

Iodice et al. [4] showed, with the addition of anhydrous ethanol in blend, torque and brake power also increase owing the heat of evaporation of ethanol (around 910 kJ / kg) is twice higher than gasoline. So, during the evaporation of ethanol / gasoline mixture under of hot operating conditions, the flow of fuel tends to absorb more cylinder heat than gasoline. In this condition, the charge and intake manifold temperatures decreases, thus increasing volumetric efficiency.

Deng et al. [3] do a research on pure gasoline and the mixture with hydrous ethanol 95,5%v. Compared to using pure gasoline, thermal brake efficiency is obtained higher when using a mixture of hydrous ethanol gasoline on the engine tested. It is caused by hydroxyl radicals (-OH) produced by ethanol, which improves the combustion and flame propagation speed. The results of the research are shown in Figure 3

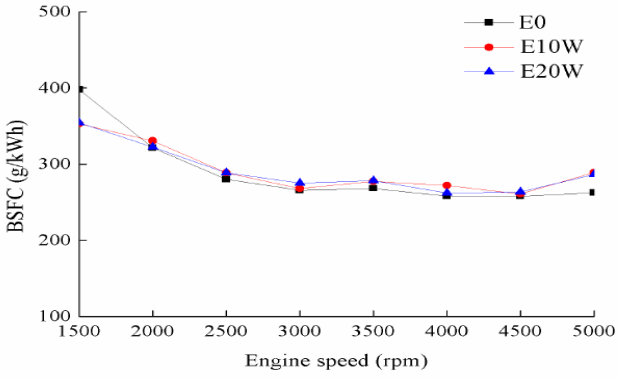

Figure 3. Effect of engine speed to BSFC using gasoline and its mixture with ethanol

Because of, a shorter combustion period the results is lower heat loss to the cylinder wall, which promotes the thermal brake efficiency. Also compared between E10W and E20W; E20W produces higher thermal brakes efficiency on the tested machine. It caused by presence of oxygen is higher at E20W, which helps increase combustion.

Costa and Sodré [15] found that it was consumed more hydrous ethanol to get the same power compared to gasoline ethanol mixture. For both types of fuel, it is operated at equivalence ratio 1.12, and the stoichiometric air/fuel ratio is 13.1 for the gasoline-ethanol blend and 8.7 for hydrous ethanol. BSFC for hydrous ethanol is up to 54% higher than that of gasoline-ethanol blend, as a consequence of the lower heating value of hydrous ethanol with respect to that of the ethanol-gasoline blend. Improved fuel economy using hydrous ethanol instead of the ethanol gasoline blend, could only be possible with engine modifications, especially in the compression ratio

Chuepeng et al. [16] stated that in stoichiometric air-fuel mixture the rate of consumption of hydrous ethanol fuel is higher than anhydrous ethanol and gasoline around 9% and 194%. The greater fuel consumption for hE100 than that of the E100 is correspondent to the lower heating value of hE100 which is lesser by approx. 5% than that of the E100.

Based on the results of previous studies that the speed of flame and better quality emissions from hydrous ethanol, the current study compares ethanol fuel (a-zeotropic 95.5% v) with anhydrous ethanol fuel (99.7% v). Tests are carried out using varying of loads on the both type of fuel.

2. Methods

The research was conducted by laboratory test methods. The first step, for anhydrous ethanol fuel is use absolute ethanol for analysis from Merck. Furthermore, the anhydrous ethanol was diluted to hydrous ethanol (a-zeotropic) at (95.5% v) water content at the analytical laboratory. For testing of power, specific fuel consumption and thermal efficiency, was tasted out on engine brake power indicator TD 800PM load cell type with a test set-up as shown in Figure 4. By processing the test data, the results of calculations are obtained as in Tables 1 and 2.

3. Results and Discussion

By using the preliminary data engine with speed of 3500 rpm, the load increases every 1 kg, 15 mm orifice diameter, 200 mm load arm length. With the use of (Torque)

$$\tau = F.r, \quad (1)$$

Fuel consumption Q_{mf} (kg/s) where:

$$Q_{mf} = Q_v.\rho_f\,, \quad (2)$$

Power produced can be calculated by using equation (3):

$$(P) = \frac{2\pi Frn}{60} \text{ in kW} \quad (3)$$

The air flow rate through the orifice plate is calculated by equation (4):

$$Q_{va} = \frac{Q_{ma}}{\rho_a} = \alpha\varepsilon\frac{\pi d^2}{4}\sqrt{\frac{2\Delta p}{\rho_a}} \quad (4)$$

and consumption of specific fuel is calculated as below:

$$B_{sfc} = \frac{Q_{mf}\left(^{kg}/_{s}\right)}{P(kW)} \quad (5)$$

Volume of combustion chamber:

$$Q_{th} = \text{engine TDV x } \frac{n}{2 \text{ x } 60}\left(\frac{m^3}{s}\right), \quad (6)$$

with volumetric efficiency:

$$\eta_v = \frac{Q_{va}}{Q_{th}} \text{ x } 100\%; \quad (7)$$

Thermal Efficiency:

$$\eta_{bt} = \frac{P(kW)}{Q_f} = \frac{P(kW)}{Q_{mf}.LHV} \quad (8)$$

So that the results of calculations are obtained as presented in Tables 1 and 2.

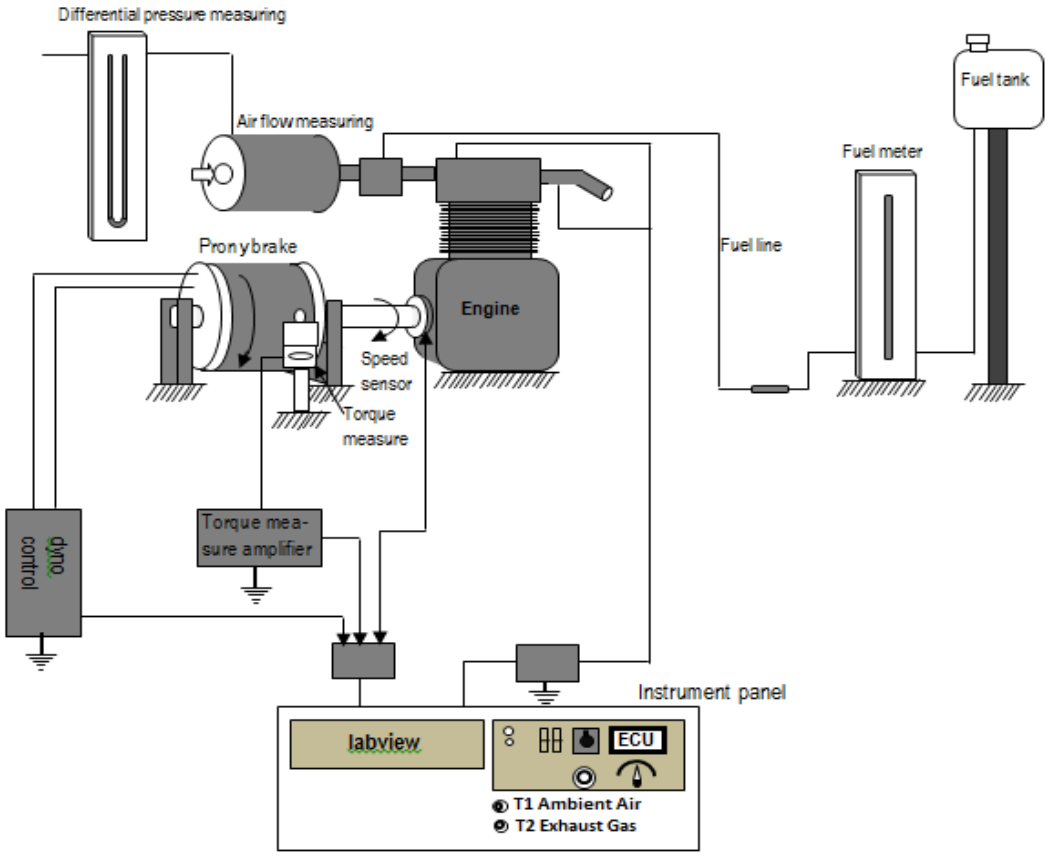

Figure 4. Set-up experimental

Table 1. Results of calculation of ethanol anhydrous data

TD 800PM SINGLE-CYLINDER ENGINE TEST-BED, Mechanical Absorber

Room temperatur : 29
Atmospheric pressure : 105,2 kPa
Opening position of throttle valve : -

Engine type : .....
Fuel type : anhydrous ethanol
Specific gravity : .....

Tested by : ..... Date :5/7/2018
Air box / Orifice diameter : 300/15
Manometer slope : 1:5
Manometer reading for zero air flow :

n rpm	Net Force kg	τ (N.m)	Fuel Consumtion					Air flow rate						A/F ratio	Temperatur (°C)		P kW	B_{sfc} kg/kWh	η_{bt} %
			Graduated cylinder			Indicator Q_f kW	Q_{mf} kg/s	Air box			Q_{th} (m^3/s)	Indicator Q_{va} m^3/s	Q_{ma} kg/s		Engine Inlet air T1	Exhaust gas T2			
			Volume ml	Time s	Q_{vf} (l/s)			Manometer Reading mm H2O											
								Left	Right	Net									
3500	0	0	5	17.62	0.00028	5.96311	0.00022418	285	115	170	0.0057	0.00161	0.0019	8.4004	28	281	0	#DIV/0!	0
3136	1	1.96	5	18.01	0.00028	5.83398	0.00021932	285	115	170	0.0051	0.00161	0.0019	8.5863	28	300	0.6443	1.22541	11.044
3100	2	3.92	5	19.11	0.00026	5.49817	0.0002067	285	115	170	0.0051	0.00161	0.0019	9.1108	28	281	1.2739	0.58414	23.169
3000	3	5.88	5	19.45	0.00026	5.40206	0.00020308	280	120	160	0.0049	0.001561	0.0018	8.996	28	282	1.8491	0.39538	34.23
2600	4	7.84	5	20.15	0.00025	5.21439	0.00019603	270	130	140	0.0042	0.001461	0.0017	8.7178	28	261	2.1368	0.33027	40.979
2313	5	9.8	5	21.18	0.00024	4.96081	0.0001865	270	130	140	0.0038	0.001461	0.0017	9.1635	28	247	2.3761	0.28255	47.898

Table 2. Results of a-zeotropic ethanol data calculation

TD 800PM SINGLE-CYLINDER ENGINE TEST-BED, Mechanical Absorber

Room temperatur : 29
Atmospheric pressure : 105,2 kPa
Opening position of throttle valve : -

Engine type : .....
Fuel type : azeotropik ethanol 95,5%v
Specific gravity : .....

Tested by : ..... Date : 5/7/2018
Air box / Orifice diameter : 300/15
Manometer slope : 1:5
Manometer reading for zero air flow :

n rpm	Net Force kg	τ (N.m)	Fuel Consumtion					Air flow rate						A/F ratio	Temperatur (°C)		P kW	B_{sfc} kg/kWh	η_{bt} %
			Graduated cylinder			Indicator	Q_{mf} kg/s	Air box				Indicator	Q_{ma} kg/s		Engine Inlet air T1	Exhaust gas T2			
			Volume ml	Time s	Q_{vf} (l/s)	Q_f kW		Manometer Reading mm H2O			Q_{th} (m^3/s)	Q_{va} m^3/s							
								Left	Right	Net									
3500	0	0	5	10.34	0.00048	9.93772	0.00038685	370	30	340	0.0057	0.002276	0.0027	6.8844	28	320	0	#DIV/0!	0
3321	1	1.96	5	10.97	0.00046	9.367	0.00036463	365	30	335	0.0054	0.002259	0.0026	7.25	29	332	0.6823	1.9238	7.2844
3244	2	3.92	5	11.23	0.00045	9.15013	0.00035619	360	30	330	0.0053	0.002243	0.0026	7.3662	29	334	1.333	0.96193	14.568
3221	3	5.88	5	11.65	0.00043	8.82026	0.00034335	360	30	330	0.0053	0.002243	0.0026	7.6417	29	337	1.9854	0.62258	22.509
3147	4	7.84	5	12.06	0.00041	8.5204	0.00033167	360	40	320	0.0051	0.002208	0.0026	7.7899	29	323	2.5863	0.46167	30.355
2575	5	9.8	5	12.94	0.00039	7.94096	0.00030912	335	55	280	0.0042	0.002066	0.0024	7.8184	29	334	2.6453	0.42068	33.312

3.1 Power

The power produced by a-zeotropic ethanol is higher than that of anhydrous ethanol at the same load. Difference increases power proportional with increased load as shown in Figure 5. Engine power performance is significantly dependent on the physical and chemical properties of the fuel used. The latent heat of a-zeotropic ethanol evaporation is lower than ethanol anhydrous. It caused by the structure of a-zeotropic ethanol molecules is shorter so it is easier to evaporate than ethanol anhydrous [7]. Therefore, produce more power in engine operation but will consume more fuel, which leads to higher volumetric efficiency. Furthermore, a-zeotropic ethanol has a centralized oxygen molecule that benefits the combustion process so that it produces more perfect combustion, and increases combustion efficiency.

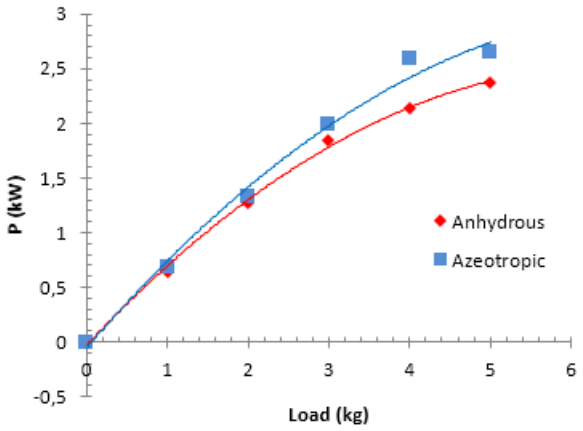

Figure 5. Comparison of the power produced by ethanol a-zeotropic with ethanol anhydrous at the same load.

A-zeotropic ethanol combustion speed higher than anhydrous ethanol causes the generated power is also higher. Seeing these factors affect engine power performance to be consideration in the use of a-zeotropic ethanol into fuel.

3.2 Specific fuel consumption

The latent heat evaporation of a-zeotropic ethanol is lower than anhydrous ethanol causes a-zeotropic ethanol to evaporate more easily in the engine operation process. The result is more fuel goes into the combustion chamber resulting in greater power. Lower heat value causes the need of more amount of fuel to produce the same power. This result consistent with [13,14]. Comparison of specific fuel consumption shown in Figure 6.

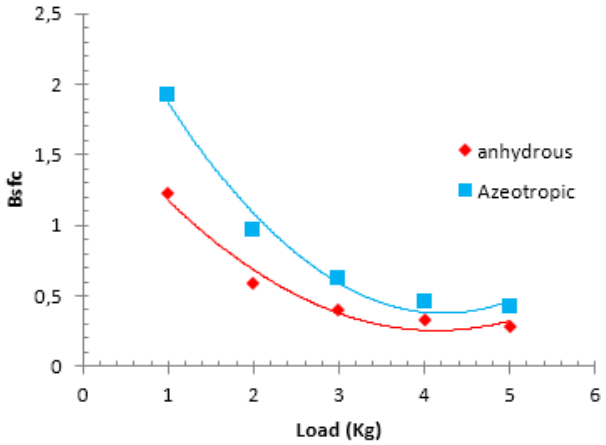

Figure 6. Comparison of specific fuel consumption using a-zeotropic ethanol and anhydrous ethanol

Hydrogen bonds in O and H atoms in ethanol and water molecules cause molecules to group with strong bonds. Thus in the process of evaporation in the carburetor the distance between fuel molecules becomes closer which implies occupying a narrower space so that more fuel enters the combustion chamber. Bigger combustion velocity of a-zeotropic ethanol is also a cause of bigger combustion power and better emission quality [3]. This is also in accordance with the results of Phuangwongtrakul's research [17]. The higher of ethanol levels BSFC is increasing.

3.3 Thermal efficiency

A-zeotropic Ethanol thermal efficiency is lower than anhydrous ethanol this caused more fuel needs to produce the same power as anhydrous ethanol. The combustion efficiency is influenced by the amount of fuel needed per cycle, the temperature in the cylinder and the homogeneity

of the mixture. Because more fuel is supplied (load increases), there is an increase in reactant stratification at higher loads. Load stratification occurs and causes over rich zona formation. So the tendency of the difference in combustion efficiency is greater according to the increase in load. This is the same as [18], the thinner the mixture the combustion efficiency increases. The increase of power when the use of a-zeotropic ethanol is smaller than the fuel consumption of each power produced. So that thermal efficiency decreases when using ethanol a-zeotropic fuel. Graphs comparing between thermal efficiency of a-zeotropic fuel and anhydrous ethanol are shown in Figure 7.

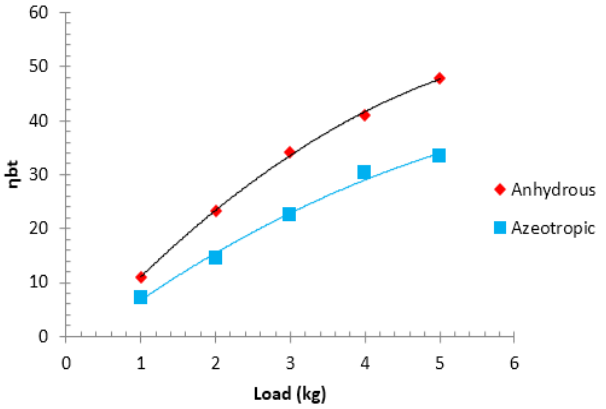

Figure 7. Comparison of thermal efficiency using a-zeotropic ethanol fuel and anhydrous ethanol

4. Conclusions

Using a-zeotropic ethanol fuel produced greater power than anhydrous ethanol at the same load. The higher the load the higher difference in power will produced. The amount of power produced depends on the characteristics of combustion such as combustion speed and volumetric efficiency of fuel.

Fuel consumption use a-zeotropic fuel higher than anhydrous ethanol fuel. This is due to the a-zeotropic ethanol fuel heating value is smaller than anhydrous ethanol or to produce the same power, consumption more amount of a-zeotropic ethanol fuel than a-zeotropic ethanol fuel.

The thermal efficiency of a-zeotropic ethanol is smaller than anhydrous ethanol at the same load. The difference in efficiency increases in proportion to the increase in load.

References

[1] I. Awad Omar, R. Mamat, M. Ali Obed, N.A.C. Sidik, T. Yusaf, K. Kadirgama and M. Kettner, "Alcohol and ether as alternative fuels in spark ignition engine", *Renewable and Sustainable Energy Review*, http://dx.doi.org/10.1016/j.rser.2017.09.074

[2] I.M. Suarta, I.N.G. Baliarta, I.P.G. Sopan Rahtika and P.W. Sunu, "The Role of Hydrogen Bonds Of The Azeotropic Hydrous Ethanol Fuel Composition To The Exhaust Emissions", *Journal of Physics*: Conf. Series 953 2018 *J. Phys.: Conf. Ser.* **953** 012070

[3] X. Deng, Z. Chen, X. Wang, H. Zhen, and R. Xie, "Exhaust noise, performance and emission characteristics of spark ignition engine fuelled withpure gasoline and hydrous ethanol gasoline blends", *Case Studies in Thermal Engineering. https://doi.org/10.1016/j.csite.2018.02.004*

[4] P. Iodice, G. Langella, A. Amoresano, "Ethanol In Gasoline Fuel Blends: Effect On Fuel Consumption and Engine Out Emissions Of Si Engines In Cold Operating", conditions. *https://doi.org/10.1016/j.applthermaleng.2017.11.090*

[5] P. Sakthivel, K.A. Subramanian, R. Mathai, "Indian scenario of ethanol fuel and its utilization in automotive transportation sector", Resources, Conservation & Recycling, 132, 2018, pp. 102–120

[6] S. Chuepeng; S. Srisuwan and M. Tongroon, "Lean hydrous and anhydrous bioethanol combustion in spark ignition engine at idle", Energy Conversion and Management 128, 2016, pp. 1–11

[7] I.M. Suarta, I.N.G. Wardana, H. Nurkholis and W. Widya, "The Role of Molecule Clustering by Hydrogen Bond in Hydrous Ethanol on Laminar Burning Velocity", *Journal of Combustion*. Article ID 5127682, 9 pages. http://dx.doi.org/10.1155/2016/5127682.

[8] J.L.S. Fagundez, R.L. Sari, F.D. Mayer, M.E.S. Martins, and N.P.G. Salau, "Determination of optimal wet ethanol composition as a fuel in spark ignition engine", *Applied Thermal Engineering* http://dx.doi.org/10.1016/j.applthermaleng.2016.10.099

[9] I.M. Suarta, I.N.G. Wardana, H. Nurkholis and W. Widya,."The Role of Hydrogen Bonding on Laminar Burning Velocity of Hydrous and Anhydrous Ethanol Fuel with Small Addition of n-Heptane", *Journal of Combustion* Volume 2016, Article ID 9093428, 8 pages http://dx.doi.org/10.1155/2016/9093428

[10] B. Baine and S. Acharya, "The effect of elevated water content on swirl-stabilized ethanol/air flames", *Fuel*, 105, 2013, pp. 90–102.

[11] I. M. Yusria, R. Mamat, G. Najafi, A. Razman, Omar I. Awad, W.H. Azmi, W. F. W. Ishak, A.I.M. Shaiful, "Alcohol based automotive fuels from first four alcohol family incompression and spark ignition engine: A review on engine performanceand exhaust emissions", *Renewable and Sustainable Energy Reviews*, 77, 2017, 169–181.

[12] M. Amirabedi; S. Jafarmadar, S. Khalilarya, "Experimental investigation the effect of Mn_2O_3 nanoparticle on theperformance and emission of SI gasoline fueled with mixture of ethanol and gasoline", Applied Thermal Engineering, 149, 2019, pp. 512–519

[13] R. Munsin, Y. Laoonual, S. Jugjai, Y. Imai, "An experimental study on performance and emissions of a small SI enginegenerator set fuelled by hydrous ethanol with high water contents up to 40%", Fuel, 106, 2013, pp. 586–592

[14] R. Salvador, C. Bringhenti, J.T. Tomita, "Characterization of an ethanol fueled heavy-duty engine powering a generator set", http://dx.doi.org/10.1016/j.applthermaleng.2016.03.107

[15] R.C. Costa, and J.R. Sodré, "Hydrous ethanol vs. gasoline-ethanol blend: Engine performance and emissions", Fuel, 89, 2010, pp. 287–293.

[16] S. Chuepeng, S. Srisuwan, and M. Tongroon, "Lean hydrous and anhydrous bioethanol combustion in spark ignition engine at idle", Energy Conversion and Management, 128, 2016, pp. 1-11.

[17] S. Phuangwongtrakul, W. Wechsatol, T. Sethaput, K. Suktang, S. Wongwises, "Experimental study on sparking ignition engine performance for optimal mixing ratio of ethanol-gasoline blended", Fuels. *http://dx.doi.org/doi: 10.1016/j.applthermaleng.2016.02.084*

[18] T. Diórdinis, M. Lanzanova, M. D. Nora and H. Zhao, "Performance and economic analysis of a direct injection spark ignitionengine fueled with wet ethanol", *Applied Energy*, 169, 2016, pp. 230–239

p-ISSN 2655-9145

JAMETECH
Journal of Applied Mechanical Engineering and Green Technology

Politeknik Negeri Bali,
Jl. Kampus, Bukit Jimbaran, Kuta Selatan, Badung
Bali - Indonesia 80364 - PO BOX 1064
Telp. (+62)361 701981 Fax. (+62)361 701128
Email: jametech@pnb.ac.id